Evaluation of the Parameter Sensitivities of a Coupled Land Surface Hydrologic Model at a Critical Zone Observatory

YUNING SHI, KENNETH J. DAVIS, AND FUQING ZHANG

Department of Meteorology, The Pennsylvania State University, University Park, Pennsylvania

CHRISTOPHER J. DUFFY

Department of Civil Engineering, The Pennsylvania State University, University Park, Pennsylvania

(Manuscript received 3 December 2012, in final form 6 September 2013)

ABSTRACT

Land surface models (LSMs) and hydrologic models are parameterized models. The number of involved parameters is often large. Sensitivity analysis (SA) is a key step to understand the complex relationships between parameters and between state variables and parameters. SA is also critical to understand system dynamics and to examine the parameter identifiability. In this paper, parameter SA for a fully coupled, physically based, distributed land surface hydrologic model, namely, the Flux–Penn State Integrated Hydrologic Model (Flux–PIHM), is performed. Multiparameter and single-parameter tests are performed to examine the three dimensions of identifiability: distinguishability, observability, and simplicity. Results show that Flux–PIHM model predictions of discharge, water table depth, soil moisture, land surface temperature, and surface heat fluxes are very sensitive to the selection of parameter values. Parameter uncertainties produce large uncertainties in hydrologic and land surface variable predictions. The van Genuchten parameters α and β and the Zilitinkevich parameter C_{zil} are the most identifiable among the 20 tested parameters. Results indicate that the land surface and the subsurface are closely coupled. Hydrologic parameters have significant influence on land surface simulations. At the same time, land surface parameters have considerable impacts on hydrologic simulations; the evapotranspiration prediction prior to a strong precipitation event is critical for initializing accurate prediction of discharge peaks. Results also show that parameter identifiability depends on seasons and canopy wetness. Parameter identifiability at high and low flow conditions can be extremely different. Complex system dynamics have been revealed during the SA.

1. Introduction

Numerical models are important tools for the forecasting of complex processes in natural systems. They can improve our understanding of those complex processes and help incorporate this understanding into decision making. Land surface models (LSMs) and hydrologic models are the numerical models designed for the forecasting and study of land surface and hydrologic processes. Overparameterization and parameter values are one of the main sources of uncertainties of hydrologic models and LSMs.

Generally, there are two types of parameters in numerical models: physical parameters and process parameters. Physical parameters are measurable parameters with physical meanings. Process parameters are those parameters that cannot be measured directly because of practical or theoretical reasons. Parameter uncertainties could be large if a process parameter is poorly defined, if a physical parameter is not accurately measured, or if a parameter is not sufficiently representative (Prihodko et al. 2008). In LSMs and hydrologic models, the physical parameter values in actual field conditions might be substantially different from those measured in the laboratory; the range of variation in parameter values could span orders of magnitude, especially in hydrologic models (Bras 1990). Some physical parameters have considerable spatial heterogeneity, which weakens the representativeness of the measured parameter values. To reduce the uncertainty in model parameters and to yield the observed system response, LSM and hydrologic model parameters need to be tuned or calibrated.

Corresponding author address: Yuning Shi, Department of Meteorology, 415 Walker Building, The Pennsylvania State University, University Park, PA 16802.
E-mail: yshi@psu.edu

DOI: 10.1175/JHM-D-12-0177.1

The calibration of LSM and hydrologic model parameters has been the focus of many studies (e.g., Gupta and Sorooshian 1985; Sellers et al. 1989; Sorooshian et al. 1993; Franchini 1996; Gupta et al. 1999; Xia et al. 2002; Wagener et al. 2003; Jackson et al. 2003; Moradkhani et al. 2005; Kollat and Reed 2006; Xie and Zhang 2010; Cammalleri and Ciraolo 2012; Yu et al. 2013).

Model sensitivity analysis (SA) is a vital step toward successful parameter estimation. Both LSMs and hydrologic models are parameterized models. Model structures are complex, and the number of involved parameters is often large. Because of the limitation of computational capabilities, optimization algorithms, and model parameterizations, not all model parameters can be estimated in complex models. SA analyzes the influence of model parameters on model predictions. Parameter estimation efforts can be guided by the results of SA.

SA is critical to understanding complex system dynamics within numerical models. It provides insights into model structures and system dynamics. The nonuniqueness of numerical model parameters and structures, that is, equifinality (Beven 1993), reveals that there exist strong interactions between model parameters. The SA provides a means to understand the complex interaction between model parameters and the relationship between state variables and parameters. SA can also guide observational system designs.

There are a number of SA methods that are available, for example, the Sobol' (1993) method, the Morris (1991) method, the nominal range method, the Fourier amplitude sensitivity test (FAST; Cukier et al. 1973, 1975, 1978), the regression method, regional sensitivity analysis (RSA; Hornberger and Spear 1981; Freer et al. 1996), and scatterplots. Those SA methods have been widely used for land surface and hydrologic models (e.g., Salehi et al. 2000; Cullmann et al. 2006; Demaria et al. 2007; Tang et al. 2007; Pappenberger et al. 2008; Hall et al. 2009; Reusser et al. 2011; Massmann and Holzmann 2012). The comparison of SA methods has been the interest of many studies (e.g., Saltelli et al. 2005; Frey and Patil 2002; Hall et al. 2009; Confalonieri et al. 2010; Reusser et al. 2011; Massmann and Holzmann 2012). Different SA methods have been found to reveal different sensitivity rankings in complex models (Campolongo and Saltelli 1997; Helton et al. 2006; Tang et al. 2007; Pappenberger et al. 2008; Sun et al. 2012). Each method has its own strengths, limitations, and demands, and no method is clearly superior to others (Frey and Patil 2002). Some methods, like the Sobol' method, are more appropriate for systems with strong nonlinearity, but are computationally expensive. Other methods, like the nominal range method and the regression method, are limited to models with strong linearity but are much less computationally intensive. Choosing the appropriate SA methods therefore depends on the goal of the SA and the computational cost of the model (Saltelli et al. 2006; Reusser et al. 2011).

The Flux–Penn State Integrated Hydrologic Model (Flux–PIHM; Shi et al. 2013a) is a coupled, physically based land surface hydrologic model that incorporates a land surface scheme into the Penn State Integrated Hydrologic Model (Qu 2004; Qu and Duffy 2007; Kumar 2009). The land surface scheme is mainly adapted from the Noah LSM (Chen and Dudhia 2001; Ek et al. 2003). Flux–PIHM was manually calibrated and evaluated at a small watershed in central Pennsylvania (Shi et al. 2013a). Manual calibration, however, is highly time consuming and labor intensive. The now widely used data assimilation method, the ensemble Kalman filter (EnKF; Evensen 1994), provides the possibility for automatic sequential calibration for complex models like Flux–PIHM, a spatially distributed, physically based, and fully coupled land surface hydrologic model. Prior to parameter estimation using EnKF, SA needs to be performed to guide the parameter estimation efforts. The large computational cost of the physically based model limits the choices of SA methods. Fortunately, the responses of hydrologic models to the variations of inputs (forcing and parameters) are often found to be nearly linear (Hall et al. 2009; Sun et al. 2012). Therefore, the SA methods for linear models are applicable to computational intensive hydrologic models (Hall et al. 2009; Sun et al. 2012) like Flux–PIHM.

Aksoy et al. (2006) used the concept of parameter identifiability as an indicator for whether or not a parameter could be estimated successfully using the EnKF. Zupanski and Zupanski (2006) and Nielsen-Gammon et al. (2010) generalized the characteristics of parameters for successful estimation as observability, simplicity, and distinguishability. Nielsen-Gammon et al. (2010) concluded these characteristics as the three dimensions of parameter identifiability. Observability describes how strongly the change of parameter values could be reflected onto observation space. High observability means that a change in parameter values could lead to a relatively large change in model predictions. Simplicity describes how smoothly model predictions vary with the change of parameter values. An ideal simplicity is that the model predictions vary monotonically with the change of parameter values. Distinguishability describes how effectively the impact of one parameter could be distinguished from other parameters. Low observability, low simplicity, or low distinguishability could make parameter estimation difficult to perform. Nielsen-Gammon et al. (2010) used a combination of the regression method (correlation coefficient ranking), the

nominal range method, and scatterplots to examine those characteristics and identified the model parameters suitable for parameter estimation. Those SA methods have been proven useful for EnKF implementation (Aksoy et al. 2006; Nielsen-Gammon et al. 2010; Hu et al. 2010) and are suitable for a model like Flux–PIHM, which has large computational cost but relatively strong linearity.

In this paper, SA analysis is performed in preparation for Flux–PIHM parameter estimation using EnKF (Shi et al. 2013b, manuscript submitted to *Water Resour. Res.*), under the framework provided by Nielsen-Gammon et al. (2010). The SA aims to select the most identifiable Flux–PIHM model parameters to be estimated using EnKF and to help interpret EnKF parameter estimation results. Complex system dynamics are revealed when examining model parameter sensitivities. By examining the sensitivity of hydrologic variables to land surface parameters and sensitivity of land surface variables to hydrologic parameters, the SA is also expected to enhance our understanding of land surface–subsurface interactions within Flux–PIHM.

2. Flux–PIHM model parameters

As a coupled land surface hydrologic model, Flux–PIHM has a high dimensional parameter space. Those parameters can be divided into hydrologic parameters and land surface parameters, depending on the module in which the parameters appear.

The hydrologic parameters included in the SA are the van Genuchten (1980) soil parameters α and β, the vertical hydraulic conductivity of infiltration layer K_{infV}, the vertical hydraulic conductivity of soil layer K_V, the vertical macropore hydraulic conductivity K_{macV}, the effective porosity Θ_e, and the riverbed roughness n_{riv}. The calibration of those parameters has been the focuses of many studies (e.g., Beven and Binley 1992; Eckhardt and Arnold 2001; Henriksen et al. 2003; Tang et al. 2006; Yu et al. 2013). The van Genuchten soil parameters α and β determine the soil water retention curve as well as the unsaturated hydraulic conductivities. The parameter α is the inverse of the air-entry value of soil, and β is the pore size distribution index. The soil water retention curve defines the saturation ratio of soil θ at different pressure heads h. In the van Genuchten (1980) equation,

$$\theta = \left[\frac{1}{1+(\alpha h)^{\beta}}\right]^{1-(1/\beta)}, \tag{1}$$

and h is assumed to be positive for simplification. The parameters K_{infV} and K_V control soil infiltration and groundwater recharge. The parameter K_{macV} could have impacts on soil infiltration and groundwater recharge, depending on the thickness of the macropore layer. The parameter Θ_e defines the water capacity of soil, and n_{riv} affects the channel flow rate. Note that the hydrologic parameters that control the horizontal groundwater flow and the water flow between the aquifer and the river channel are not included in the SA. The calibration of those parameters is performed by matching the modeled and observed discharge recession curves and water table depths. Those parameters can be relatively accurately determined using only a few observations; therefore, they can be excluded from the SA to reduce the parameter dimension. The values of those parameters are set to their manually calibrated parameter values as in Shi et al. (2013a).

The land surface parameters included in the SA are the Zilitinkevich (1995) parameter C_{zil}, the reference visible solar radiation R_{gl}, the water vapor exchange coefficient h_s, the reference temperature T_{ref}, the field capacity Θ_{ref}, the soil wilting point Θ_w, the soil evaporation coefficient fx_s, the canopy evaporation coefficient fx_c, the surface albedo A, the reference canopy water capacity S, and the reference drip rate k_D. The Zilitinkevich parameter C_{zil} affects the ratio between the roughness length for heat (moisture) and the roughness length for momentum, which in turn affects the surface exchange coefficients for heat and momentum (Chen et al. 1997). Zilitinkevich (1995) formulates the ratio between the roughness length for heat and the roughness length for momentum as a function of the roughness Reynolds number:

$$\frac{z_{0\mathrm{m}}}{z_{0\mathrm{t}}} = \exp\left(kC_{\mathrm{zil}}\sqrt{\mathrm{Re}^*}\right), \tag{2}$$

where $z_{0\mathrm{m}}$ is the roughness length for momentum, $z_{0\mathrm{t}}$ is the roughness length for heat, and $k = 0.4$ is the von Kármán constant. Parameter Re* is the roughness Reynolds number formulated as

$$\mathrm{Re}^* = \frac{u_0^* z_{0\mathrm{m}}}{\upsilon}, \tag{3}$$

where u_0^* is the surface friction velocity, and υ is the kinematic molecular viscosity. Transpiration is constrained by the canopy resistance (R_c), which is affected by photosynthetically active radiation (PAR), air temperature, air humidity, and soil moisture. Impacts of those environmental forcing variables are modulated by parameters R_{gl}, h_s, T_{ref}, Θ_{ref}, and Θ_w:

$$R_c = \frac{R_{\mathrm{cmin}}}{\mathrm{LAI}\times F_1F_2F_3F_4}, \tag{4}$$

$$F_1 = \frac{(R_{\text{cmin}}/R_{\text{cmax}}) + f}{1+f}, \quad \text{where} \quad f = 0.55\frac{S\downarrow}{R_{\text{gl}}}\frac{2}{\text{LAI}}, \tag{5}$$

$$F_2 = \frac{1}{1 + h_s(q_s - q)}, \tag{6}$$

$$F_3 = 1 - 0.0016(T_{\text{ref}} - T_a)^2, \tag{7}$$

and

$$F_4 = \sum_{i}^{N_{\text{root}}} \frac{(\Theta_i - \Theta_w)d_{z_i}}{(\Theta_{\text{ref}} - \Theta_w)d_{\text{root}}}, \tag{8}$$

where F_1, F_2, F_3, and F_4 represent impacts from PAR, vapor pressure deficit, air temperature, and root zone soil moisture, respectively, and are constrained in the range (0, 1]. Here $R_{\text{cmax}} = 5000\,\text{s}\,\text{m}^{-1}$ is the cuticular stomatal resistance (Dickinson et al. 1993), LAI is the leaf area index, $S\downarrow$ is the downward solar radiation, q is the specific humidity of air, q_s is the saturation specific humidity at air temperature, T_a is the air temperature, N_{root} is the total number of soil layers containing root, d_{z_i} is the thickness of the ith soil layer, and d_{root} is the total depth of root zone. Soil evaporation is affected by parameters Θ_{ref}, Θ_w, and fx_s:

$$E_{\text{soil}} = (1 - \sigma_f)\left(\frac{\Theta_1 - \Theta_w}{\Theta_{\text{ref}} - \Theta_w}\right)^{fx_s} E_p, \tag{9}$$

where σ_f is the vegetation fraction, Θ_1 is the volumetric soil moisture of the top soil layer, and E_p is the potential evapotranspiration. The canopy evaporation coefficient fx_c influences canopy evaporation and transpiration. The canopy evaporation is calculated as

$$E_c = \sigma_f E_p \left(\frac{W_c}{W_{\text{cmax}}}\right)^{\text{fx}_c}, \tag{10}$$

where W_c is the storage of canopy interception, W_{cmax} is the maximum canopy water capacity, and fx_c is the canopy evaporation coefficient. The canopy transpiration is determined by

$$E_t = \sigma_f E_p B_c \left[1 - \left(\frac{W_c}{W_{\text{cmax}}}\right)^{\text{fx}_c}\right], \tag{11}$$

where B_c is a function of canopy resistance (R_c). The reference canopy capacity S has impacts on both maximum canopy interception storage and canopy drip. Canopy drip is also affected by the reference drip rate k_D. The maximum canopy interception is formulated as

$$W_{\text{cmax}} = S \times \text{LAI}, \tag{12}$$

where S is the reference canopy water capacity. The canopy drip rate

$$\text{Dr} = \begin{cases} k_D \exp\left(b\dfrac{W_c}{W_{\text{cmax}}}\right), & 0 < W_c \le W_{\text{cmax}}, \\ k_D \exp(b) + \dfrac{W_c - W_{\text{cmax}}}{\Delta t}, & W_c > W_{\text{cmax}}, \end{cases} \tag{13}$$

where Δt is the model time step. The surface albedo A determines what proportion of solar radiation is reflected by the land surface. A complete list of the twenty potentially identifiable parameters picked out for the SA is presented in Table 1.

3. The ensemble Kalman filter

The EnKF (Evensen 1994) is a widely used data assimilation technique, which combines observations and model forecasts to produce the optimal estimate of the state of the system. The EnKF is a modified version of the Kalman filter (KF; Kalman 1960), and it estimates the model background error covariance structure by performing an ensemble of model runs based on the Monte Carlo method. It was first developed for dynamic state estimation and was later applied to model parameter estimation (e.g., Aksoy et al. 2006; Hu et al. 2010; Cammalleri and Ciraolo 2012). In the EnKF, the posterior estimate of states and parameters $\mathbf{x}^a$ is given by

$$\mathbf{x}^a = \mathbf{x}^f + \mathbf{K}(\mathbf{y} - \mathbf{H}\mathbf{x}^f), \tag{14a}$$

and the analysis error covariance is given by

$$\mathbf{P}^a = (\mathbf{I} - \mathbf{K}\mathbf{H})\mathbf{P}^f, \tag{14b}$$

where $\mathbf{x}^f$ is the prior estimate, $\mathbf{P}^f$ is the forecast background error covariance, $\mathbf{y}$ is the observation vector, $\mathbf{H}$ is the observation operator that maps state variables onto observations, $\mathbf{I}$ is the identity matrix, and $\mathbf{K}$ is the Kalman gain matrix defined as

$$\mathbf{K} = \mathbf{P}^f\mathbf{H}^{\text{T}}(\mathbf{H}\mathbf{P}^f\mathbf{H}^{\text{T}} + \mathbf{R})^{-1}, \tag{15}$$

where $\mathbf{R}$ is the observation error covariance. The EnKF can be used for parameter estimation by expanding the vector of state variable $\mathbf{x}$ to include model parameters. It has been proven efficient in the parameter estimation of conceptual hydrologic models (Moradkhani et al. 2005; Xie and Zhang 2010; Lü et al. 2013) and is promising for

TABLE 1. Flux–PIHM model parameters for the SA with their a priori parameter values and the plausible ranges of their calibration coefficients. The references are 1) Beven and Binley (1992), 2) Chen et al. (1997), 3) Gupta et al. (1999), 4) Eckhardt and Arnold (2001), 5) Anderton et al. (2002), 6) Henriksen et al. (2003), 7) Jackson et al. (2003), and 8) Tang et al. (2006).

Parameter	A priori value					Plausible range of calibration coefficient	Reference
	Soil Type						
	Weikert	Berks	Rushtown	Blairton	Ernest		
K_{infV} (m day^{-1})	18.11	9.09	5.20	0.87	3.93	0.01–100	1, 3, 5, 6, 8
K_V (m day^{-1})	5.89	0.89	1.15	0.26	0.86	0.01–100	1, 3, 5, 6, 8
K_{macV} (m day^{-1})	1811.00	909.00	520.00	87.00	393.00	0.01–100	
Θ_e (m^3 m^{-3})	0.48	0.32	0.33	0.29	0.34	0.3–1.2	1, 3
α (m^{-1})	2.46	2.51	2.84	2.79	3.27	0–2.5	5, 8
β (–)	1.20	1.21	1.33	1.33	1.32	0.95–2.5	5, 8
Θ_{ref} (m^3 m^{-3})	0.41	0.32	0.29	0.28	0.31	0.8–1.2	
Θ_w (m^3 m^{-3})	0.09	0.07	0.06	0.06	0.07	0–1.0	
	Vegetation Type						
	Deciduous forest		Evergreen forest		Mixed forest		
A (–)	0.17		0.12		0.21	0.8–1.2	3, 7
R_{cmin} (s m^{-1})	100		150		125	0.3–1.2	3, 7
R_{gl} (W m^{-2})	30		30		30	0.8–3.0	
h_s (–)	54.53		47.35		51.93	0.8–1.5	
n_{riv} (s m$^{-1/3}$)	0.04					0.5–200	6, 8
K_{rivV} (m day^{-1})	1.00					0.01–100	1, 3, 5, 6, 8
T_{ref} (°C)	24.82					0.8–1.2	
C_{zil} (–)	0.10					0.1–10	2
fx_s (–)	1.00					0.8–2.2	
fx_c (–)	0.50					0.8–1.5	
k_D (m day^{-1})	5.65×10^{-2}					0–5	
S (mm)	0.20					0–5	4, 7

the parameter estimation of physically based models such as Flux–PIHM because of its relatively simple conceptual formulation, relative ease of implementation, and affordable computational requirements.

4. Experimental design

The experiment site is the Shale Hills watershed in central Pennsylvania (Fig. 1). The Susquehanna Shale Hills Critical Zone Observatory (SSHCZO) now exists in this watershed. A real-time hydrologic monitoring network (RTHnet) is operating in SSHCZO. The Shale Hills watershed is a small-scale (0.08 km^2), V-shaped, forested catchment, characterized by relatively steep slopes and narrow ridges. Surface elevation varies from 256 m above sea level at the watershed outlet to 310 m above sea level at the ridge top. A first-order stream forms within the watershed. Five soil series have been identified within the watershed (Lin 2006; Lin and Zhou 2008), which is covered by deciduous forest, evergreen forest, and mixed forest.

The same domain setup and meteorological forcing as in Shi et al. (2013a) are adopted in this study. Considering the availability and importance of different observations, the following observable variables are chosen to test the identifiability of model parameters:

1) outlet discharge rate (Q);
2) water table depth at RTHnet wells (WTD), which is represented by the water table depth from the grid surrounded by the RTHnet wells;
3) integrated soil moisture content over the soil column at RTHnet wells (SWC);
4) land surface temperature averaged over the model domain (T_{sfc});
5) sensible heat flux averaged over the model domain (H);
6) latent heat flux averaged over the model domain (LE); and
7) canopy transpiration averaged over the model domain (E_t).

The locations for the outlet discharge gauge and the RTHnet wells are presented in Fig. 1.

Observations of the outlet discharge rate, water table depth, integrated soil moisture, and sensible and latent heat fluxes are already available at SSHCZO and have been used for manual model calibration (Shi et al. 2013a). Although the transpiration rate observations are not yet

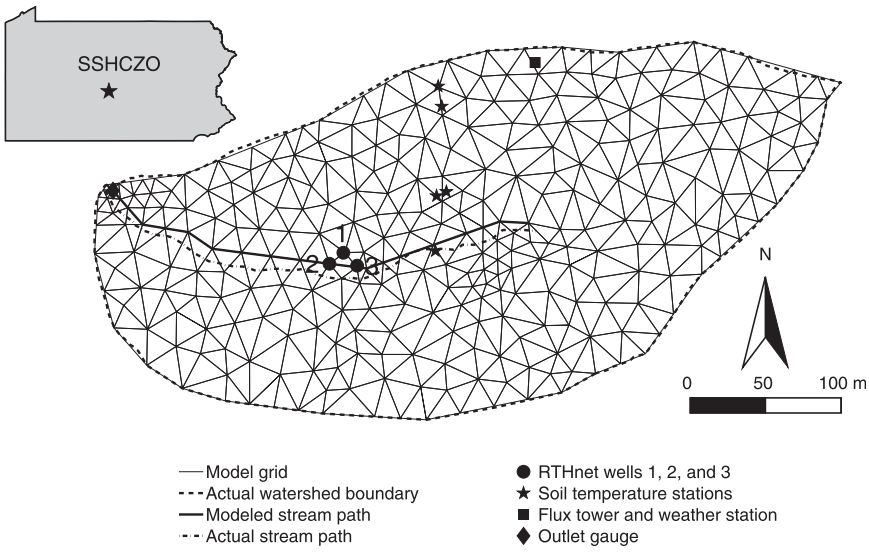

FIG. 1. Grid setting for the Shale Hills watershed model domain. The watershed boundary, the stream path, and the locations of RTHnet measurements used in this study are shown (see Fig. 2 in Shi et al. 2013a).

available, sap flux measurements have been collected at SSHCZO and can be used to estimate the canopy transpiration rate. Land surface skin temperature is not measured at SSCZHO yet. It is included because the assimilation of land surface temperature has been proven valuable for land surface simulations (e.g., Anderson et al. 1997; Crow and Wood 2003; Reichle et al. 2010), and land surface temperature can be obtained through remote sensing techniques.

To decrease the dimensionality of parameter space in Flux–PIHM, the single global calibration multiplier method (also called the one-factor method; Pokhrel and Gupta 2010; Wallner et al. 2012) is adopted. The global calibration multiplier, that is, the calibration coefficient, acts on the corresponding soil- or vegetation-related parameters for all soil or vegetation types. By applying global calibration coefficients, the dimension of parameter space is reduced and the ratios between uncalibrated a priori parameters of different soil/vegetation types are preserved. The physically plausible ranges of those model parameter values are obtained from previous studies (e.g., Beven and Binley 1992; Chen et al. 1997; Gupta et al. 1999; Eckhardt and Arnold 2001; Anderton et al. 2002; Henriksen et al. 2003; Vrugt et al. 2003; Jackson et al. 2003; Tang et al. 2006) as well as the experience from manual calibration (Shi et al. 2013a). The range of parameter values is then mapped to the range of the corresponding calibration coefficient, taking into account the parameter values for different soil or vegetation types. The a priori values and the plausible ranges of the calibration coefficients of the tested parameters at the Shale Hills watershed are presented in Table 1.

The SA is designed to select the Flux–PIHM model parameters with high identifiability for parameter estimation using EnKF. The observability, simplicity, and distinguishability of model parameters are examined. As in the work by Nielsen-Gammon et al. (2010), two sets of tests are performed in this study. One is a multiparameter test (global SA), in which all potentially identifiable parameters in Table 1 are perturbed simultaneously within their plausible ranges. The other is a set of single-parameter tests [one-at-a-time (OAT) sampling], in which only one parameter is perturbed with the other parameters set to their default values, which are the manually calibrated parameter values as in Shi et al. (2013a).

Correlation between parameters and observable variables from the multiparameter test is a good indicator of parameter distinguishability (Nielsen-Gammon et al. 2010). The correlation also indicates the likely efficiency of the assimilated observations (Hacker and Snyder 2005). EnKF updates parameter values using the covariance between model parameters and model state variables [Eq. (14)]. Low correlation between model parameters and model variables leads to small Kalman gain, which indicates that the assimilation of the observation has little impact on parameter estimation. Consequently, model parameters that have low correlations with model predictions cannot be updated effectively by EnKF. A total number of 100 Flux–PIHM model runs are performed for the multiparameter test, and the

correlation coefficients between model parameters and observable variables are used to examine parameter distinguishability. We have examined the convergence of the root-mean-square deviations (RMSDs) of observable variables, and the correlations between model parameters and observable variables, with respect to the number of ensemble members. The correlations between parameters and variables generally converge when the number of ensemble members is larger than about 50, while the variable RMSDs converge even faster. Therefore, 100 runs are sufficient for our multiparameter test. Because the main goal of the SA is to select Flux–PIHM model parameters with high identifiability, performing single-parameter tests for those parameters with low distinguishability is hardly beneficial. Therefore, the multiparameter test is performed first to examine parameter distinguishability. Parameters with relatively high correlations with observable variables, that is, parameters with high distinguishability, are selected for single-parameter tests.

In single-parameter tests, an ensemble group with a total of 10 Flux–PIHM model runs is performed for each distinguishable parameter. The nominal range method is used to examine parameter observability. RMSDs of predicted variables from different ensemble groups represent observability of model parameters (Nielsen-Gammon et al. 2010). RMSDs are calculated as

$$\mathrm{RMSD} = \sqrt{\frac{\sum_{i=1}^{N} (x_i - \overline{x})^2}{N}}, \tag{16}$$

where x_i is the model prediction of the observable variable x from the ith ensemble member, $\overline{x}$ is the average of model predictions from all ensemble members, and N is the total number of ensemble members. RMSDs produced by different parameters in single-parameter tests are compared. Small RMSDs indicate that the change of the model parameter value within the plausible range has little influence on model forecast. To try to update those parameters is not effective. Thus, the RMSDs for each observable variable from each ensemble group are compared to find parameters with high observability.

Simplicity can be addressed using scatterplots by plotting model state variables as functions of model parameters. Low simplicity would make it difficult for EnKF to find the optimal values for the model parameters. It is preferred if state variables vary monotonically with the change of parameter values. The observable variables are plotted as functions of those distinguishable and observable parameters to examine simplicity. Both multiparameter test results and single-parameter test results are used to examine simplicity.

For the multiparameter test, calibration coefficients of those 20 potentially identifiable parameters in Table 1 are randomly perturbed within their plausible ranges. The EnKF assumes that the priors have a Gaussian distribution. The calibration coefficients c are thus randomly drawn from a Gaussian distribution, with a mean of $0.5(c_{\min} + c_{\max})$ and a standard deviation of $\sigma = 0.2(c_{\min} - c_{\max})$, where $c_{\min}$ and $c_{\max}$ are the lower and upper boundaries of the plausible range. Without further information of optimal parameter values, the center of the plausible range represents the best first guesses that can be made. For a model with strong linearity, the choices of the Gaussian mean and standard deviation are not expected to strongly affect the sensitivity results. Because the plausible ranges for K_{infV}, K_V, K_{macV}, K_{rifV}, n_{riv}, and C_{zil} span orders of magnitude, a logarithmic scheme is used. Values of log$c$ are randomly drawn from a Gaussian distribution with a mean of $0.5(\log c_{\max} + \log c_{\min})$ and a standard deviation of $0.2(\log c_{\min} - \log c_{\max})$. Those calibration coefficients are transformed to log space to ensure that the lower end of the plausible range of values is sampled with more density than would be the case for a linear distribution.

Examining the correlation among input parameters is important when generating the ensemble members (Helton et al. 2006). Most of the SA methods (e.g., Sobol', FAST, and regression-based methods) require independent inputs (Saltelli et al. 2000, 2005; Jacques et al. 2006; Demaria et al. 2007). If two or more parameters are highly correlated, it would be almost impossible to distinguish their effects on model variables. It is therefore important to ensure that each model parameter varies relatively independently. We ensure that the correlation between any two calibration coefficients in our ensemble is less than or equal to 0.25.

In single-parameter tests, the calibration coefficient values for different ensemble members are evenly distributed within their plausible ranges. For the kth ensemble member, $c_k = c_{\min} + k(c_{\max} - c_{\min})/(N + 1)$, where N is the number of total ensemble members. The model run period is from 0000 UTC 15 February to 0000 UTC 1 August 2009 with a model time step of 1 min and an output interval of 1 h for every Flux–PIHM run. The period from 0000 UTC 15 February to 0000 UTC 1 March is used as model spinup period. The results from 1 March to 1 August are analyzed.

5. Results

For the sake of clarity, the parameter symbols are used to represent their calibration coefficients in this section.

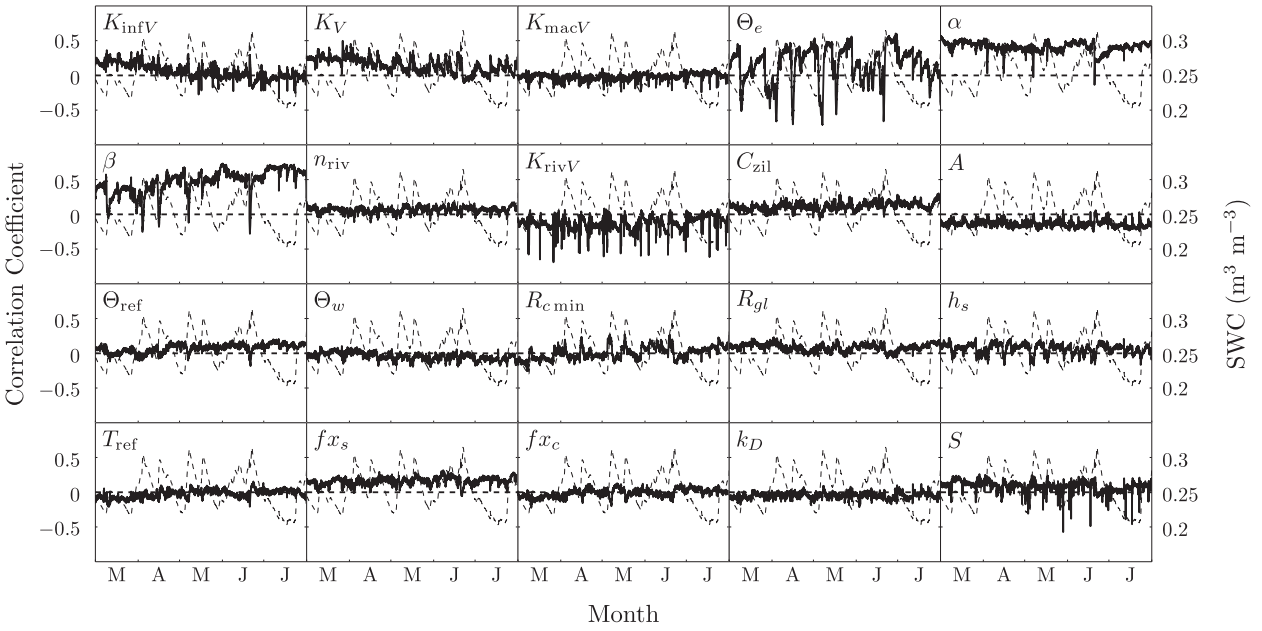

FIG. 2. Correlation coefficients between 20 potentially identifiable Flux–PIHM parameters and modeled hourly outlet discharge from the multiparameter test for March–July. The correlations plotted are the correlations among the ensemble members at each time step. The ensemble mean of SWC is plotted for reference purpose.

a. Distinguishability

The correlations between model parameters and observable variables in the multiparameter test are calculated. For hydrologic parameters, all time steps are included to calculate the correlations. For land surface parameters, however, only the midday (1700 UTC) time steps are included to filter out the diurnal cycles. We choose the midday time steps because the midday land surface fluxes have the strongest correlation with model parameters. The correlations between 20 model parameters and different observable variables are presented in Figs. 2–8. Here we define wet periods as the time periods with precipitation, typically with rising soil moisture, rising water table, and a wet canopy and dry periods as the time periods with no precipitation, typically with decreasing soil moisture, decreasing water table, and a dry canopy. The wet and dry periods defined here usually have time scales of several days. The ensemble mean of predicted SWC is plotted in Figs. 2–8 to indicate wet and dry periods.

Figures 2–8 show that the van Genuchten parameters α and β and the Zilitinkevich parameter C_{zil} are the most distinguishable among all parameters. The van Genuchten parameters show high correlations with almost every observable variable, especially Q, WTD, SWC, LE, and E_t. Parameter C_{zil} is the most dominant in T_{sfc} and H predictions. Among the four observable land-surface variables, variables LE and E_t are more moisture driven, while T_{sfc} and H are more energy driven. Results from Figs. 2–8 indicate that the van Genuchten parameters are the most distinguishable and sensitive parameters for hydrologic variables and moisture-driven land surface variables and that C_{zil} is the most distinguishable parameter for energy-driven variables.

Parameters Θ_e, α, and β are the most distinguishable and influential parameters in the prediction of discharge (Fig. 2). The correlations between those parameters and model discharge are highly time dependent, especially for Θ_e. During low flow periods (dry periods), Θ_e is positively correlated with discharge rates, while for discharge peaks, Θ_e is negatively correlated with discharge rates. The role of Θ_e is to define the available water storage of soil. Discharge at low flow periods, that is, base flow, comes from lateral groundwater flow. Larger Θ_e leads to more water storage, and thus, larger lateral groundwater volumetric flow at low flow periods. In contrast, peak flow mostly consists of surface runoff. Smaller Θ_e leads to less water storage and thus faster saturation and larger surface runoff. As a result, Θ_e is positively correlated with discharge during low flow periods, but negatively correlated with discharge at peak flows. Parameters α and β consistently show high correlations with discharge, except at those discharge peaks. Parameter S shows considerable correlation with discharge at discharge peaks, but low correlation for most of the time.

For WTD and SWC (Figs. 3, 4), α and β are also the most highly correlated parameters, but the correlations

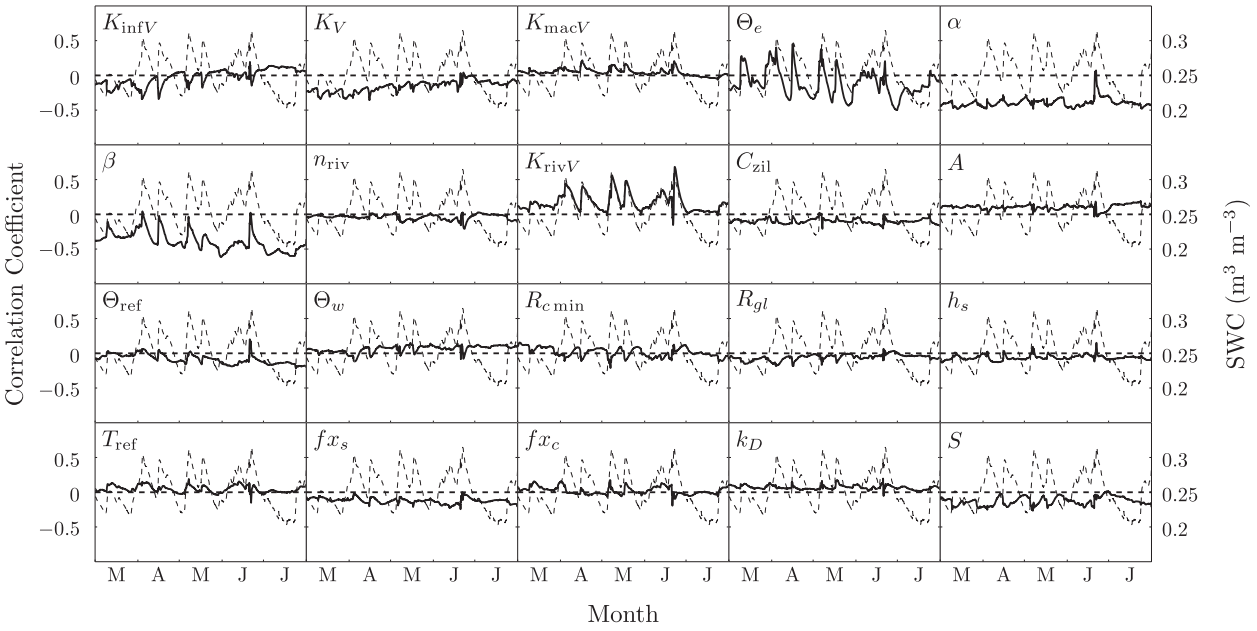

FIG. 3. As in Fig. 2, but for water table depth at RTHnet wells.

decrease at wet periods, suggesting that the peaks in SWC and drops in WTD might be controlled by the meteorological forcing, for example, precipitation, or some other model parameters. Parameters K_{infV} and K_{rivV} show high correlations with WTD during wet periods because of their roles in vertical water transport. The time series of correlation coefficients for discharge and WTD are very similar (Figs. 2, 3). For each parameter, the two time series for discharge and WTD are almost symmetric with respect to the axis of zero correlation, although time series for discharge has more high-frequency changes (Figs. 2, 3). Flux–PIHM simulation shows that at the Shale Hills watershed, 83% of total discharge is attributed to lateral groundwater flow in the year 2009. The change of water table depth near the stream is therefore highly correlated with the change of discharge rate.

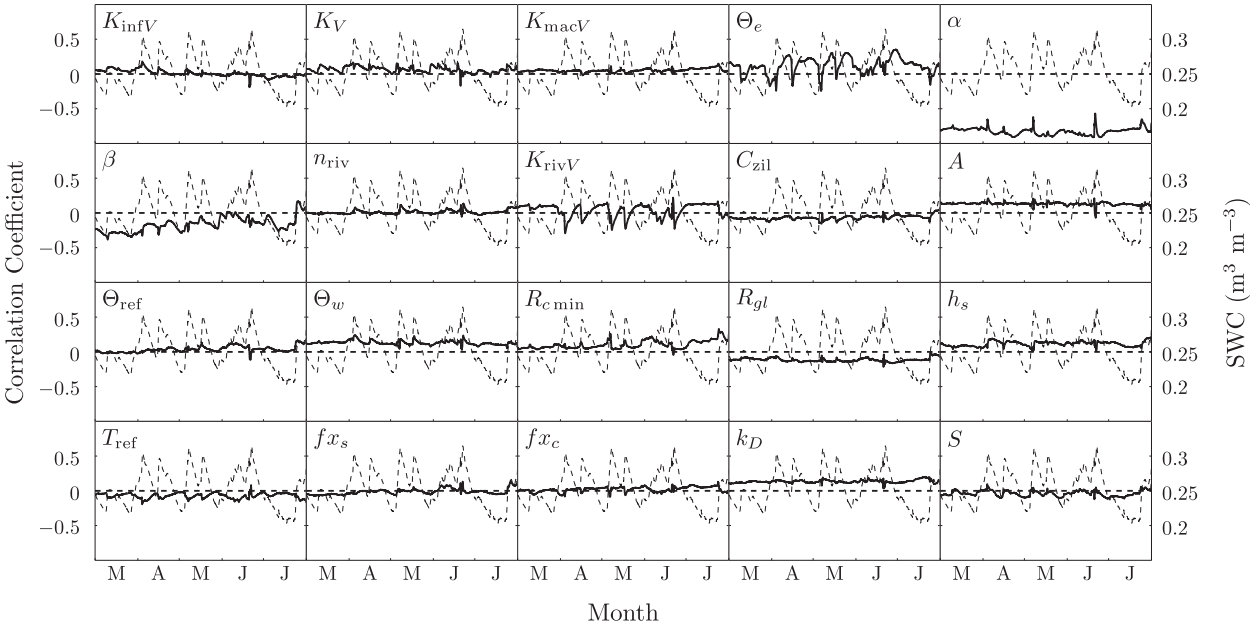

FIG. 4. As in Fig. 2, but for soil water content at RTHnet wells.

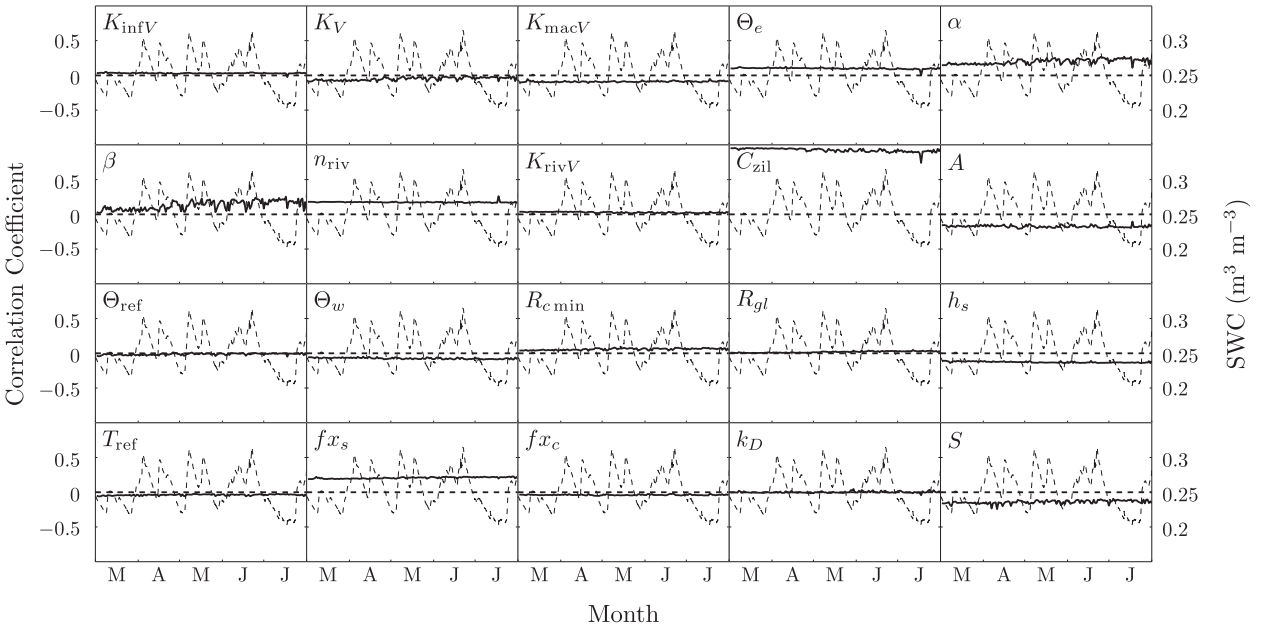

FIG. 5. As in Fig. 2, but for midday (1700 UTC) skin temperature.

The parameter C_{zil} shows a very high correlation (nearly 1.0) with the surface skin temperature, while the distinguishability of other parameters are relatively low (Fig. 5). Because of the explicit role of surface exchange coefficients in sensible heat flux formulation, C_{zil} shows high correlation with the sensible heat flux as well (Fig. 6). The influences of α and β on T_{sfc} and H get increasingly important from spring to summer (Figs. 5, 6). The influences of those two parameters on sensible heat flux are indirect and are made by affecting evapotranspiration and thus surface energy balance. During the leaf-off season (spring), the evapotranspiration rate is small; thus, the influences of α and β on surface energy balance are weak. In summer, when evapotranspiration is strong, the influences of α and β on surface energy balance get stronger.

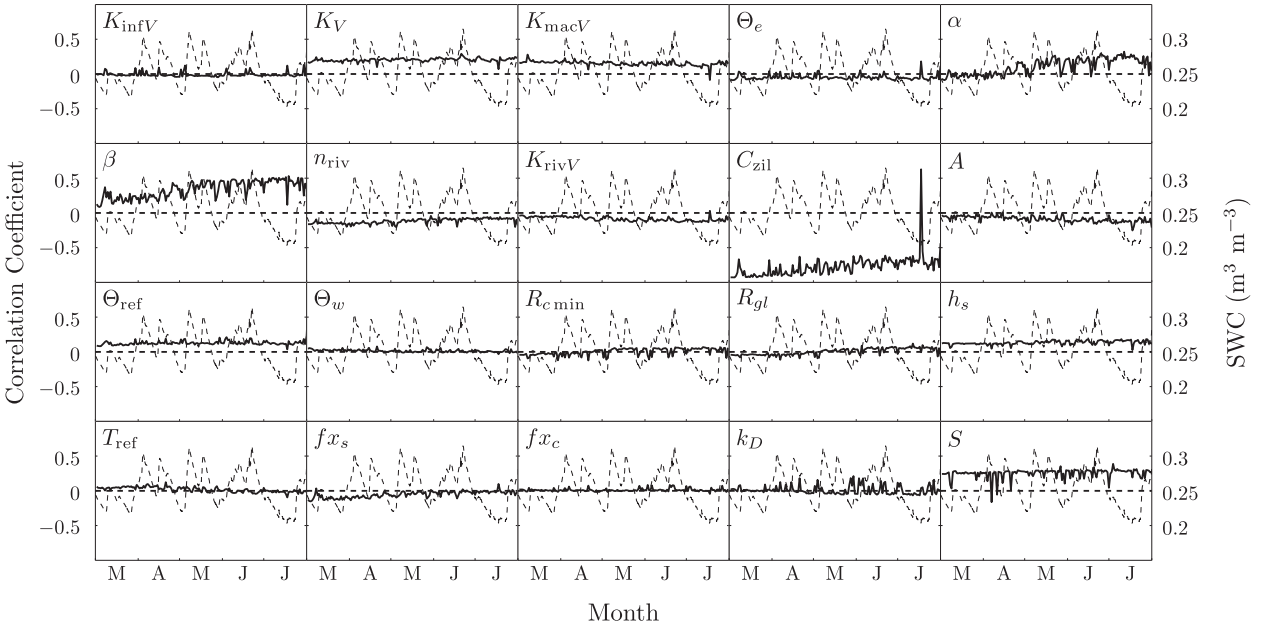

FIG. 6. As in Fig. 2, but for midday (1700 UTC) sensible heat flux.

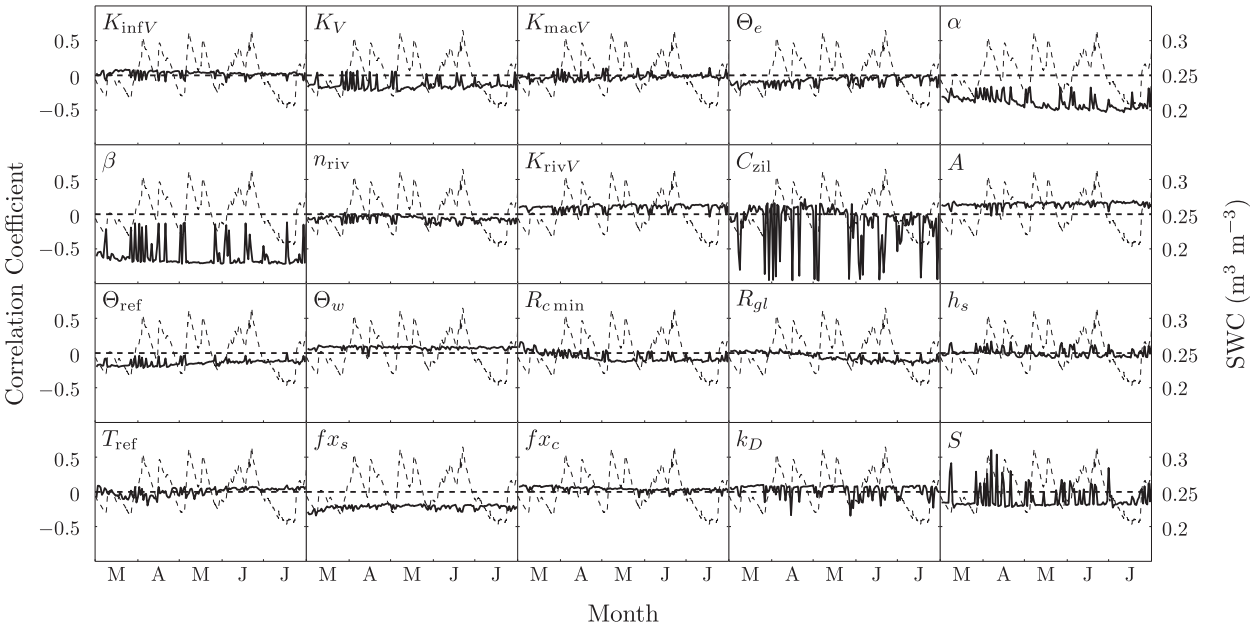

FIG. 7. As in Fig. 2, but for midday (1700 UTC) latent heat flux.

Both subsurface and land surface parameters show strong impacts on latent heat flux predictions, and their roles change with seasonality. Impacts of α and β on latent heat flux are stronger than on sensible heat flux (Figs. 6, 7) because their influences are more direct on moisture-driven variables. The correlations between those two parameters and LE also get stronger in summer than in spring. Impacts of α and β are stronger in dry periods than in wet periods. In wet periods, influences of C_{zil} and S are significant. The actual evapotranspiration is a fraction of potential evapotranspiration and can be written as

$$E = f(\Theta, T_a, S\downarrow, \Delta q, \ldots)E_p, \tag{17}$$

where E_p is the potential evapotranspiration and f is a function of soil moisture Θ, air temperature T_a, solar

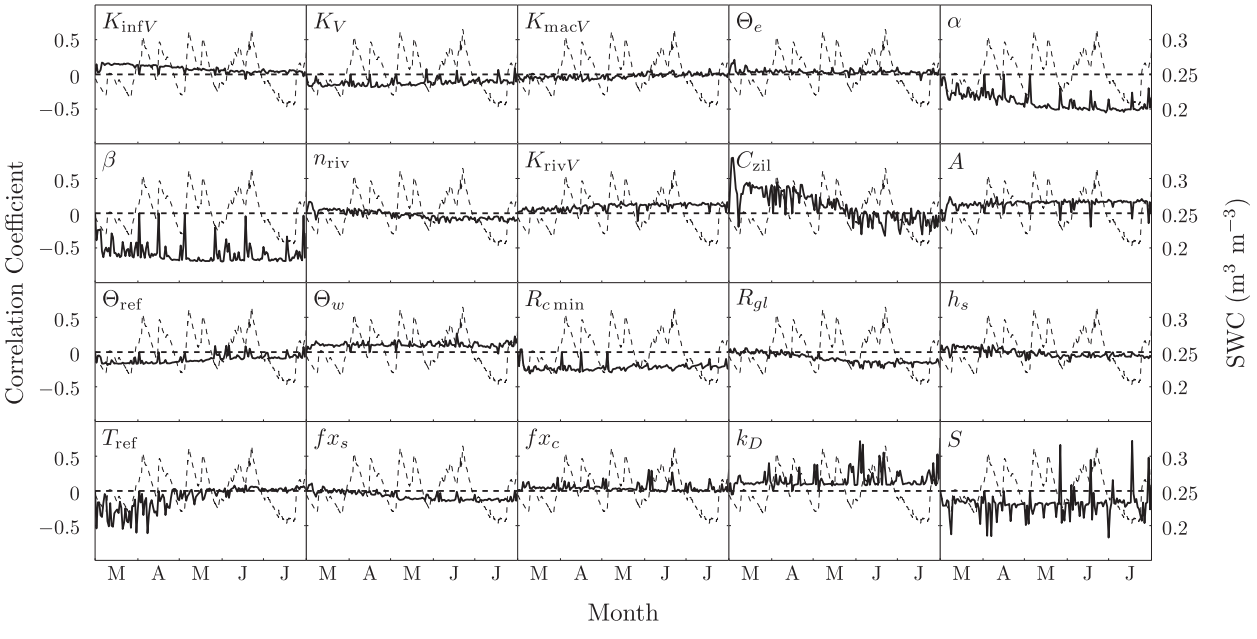

FIG. 8. As in Fig. 2, but for midday (1700 UTC) transpiration.

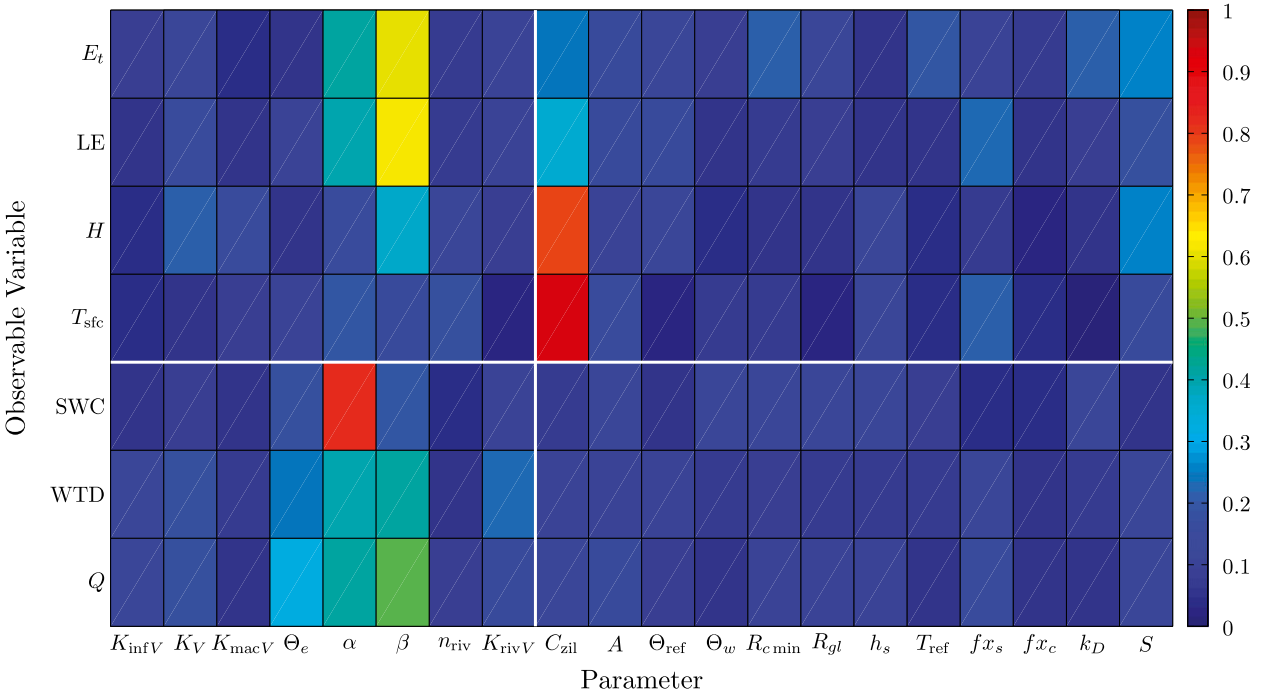

FIG. 9. RMSCs between 20 potentially identifiable Flux–PIHM parameters and different observable variables. The horizontal (vertical) white lines divide observable variables (parameters) into hydrologic and land surface variables (parameters).

radiation $S\downarrow$, water vapor deficit Δq, etc. The parameter C_{zil} affects E_p, while α and β influence the function f. Different sensitivities between dry and wet periods suggest that during wet periods, evapotranspiration is mostly determined by potential evapotranspiration, whereas during dry periods, evapotranspiration is mostly constrained by the function f. The parameter S has strong influence when the canopy is wet. Parameter fx_s, which controls the rate of soil evaporation, shows consistent correlation around -0.25 with latent heat flux.

Effects of α and β on transpiration are similar to their effects on latent heat flux (Fig. 8). Because canopy evaporation and transpiration are competing processes, parameters k_D and S, which control the canopy evaporation, are highly distinguishable when the canopy is wet. The parameter R_{cmin} shows consistent correlation around -0.25 with transpiration. The correlation between T_{ref} and transpiration reaches about -0.5 in spring, but is close to 0 in summer. The seasonal change of the correlation between T_{ref} and transpiration suggests that spring transpiration at the Shale Hills watershed is strongly constrained by air temperature stress on canopy resistance, but the constraint gets weaker in summer.

While Figs. 2–8 examine the correlation between model parameters and observable variables at each time step, the overall distinguishability during the whole experiment period needs to be quantified. Figures 2–8 show that the correlation between model parameters and observable variables is highly seasonality dependent and event based. To evaluate the overall correlation within the experiment period, a root-mean-squared correlation coefficient (RMSC) is calculated as

$$\mathrm{RMSC} = \sqrt{\frac{\sum_t (\rho_t)^2}{T}}, \tag{18}$$

where ρ_t is the correlation coefficient between model parameter and observable variables at time step t and T is the total number of time steps. The RMSCs between all parameters and observable variables are presented in Fig. 9 and Table 2.

Figure 9 shows that parameters α, β, and C_{zil} all have RMSCs larger than 0.5 with one or more observable variables. Effects of those parameters are highly distinguishable in the multiparameter test, which suggests those parameters are the most influential parameters in Flux–PIHM and might also be highly observable. Low distinguishability, however, is not necessarily equivalent to low observability. Because of the interaction of model parameters, the effects of some parameters might be compensated by the effects of other parameters, as suggested by model equifinality (Beven 1993). Thus, observability needs to be tested with single-parameter tests.

TABLE 2. RMSCs between 20 potentially identifiable Flux–PIHM parameters and different observable variables in the multiparameter test and single-parameter tests. The first number in each box indicates the RMSC in the multiparameter test and the second number indicates the RMSC in single-parameter tests. RMSCs > 0.2 in the multiparameter test are boldfaced.

	Q		WTD		SWC		T_{sfc}		H		LE		E_t	
K_{infV}	0.12	—	0.11	—	0.05	—	0.03	—	0.04	—	0.05	—	0.09	—
K_V	0.18	0.62	0.17	0.67	0.08	0.68	0.06	0.85	**0.21**	0.86	0.16	0.85	0.13	0.74
K_{macV}	0.05	—	0.07	—	0.06	—	0.09	—	0.16	—	0.05	—	0.04	—
Θ_e	**0.33**	0.85	**0.24**	0.88	0.17	0.88	0.10	0.74	0.06	0.74	0.09	0.75	0.05	0.79
α	**0.41**	0.89	**0.39**	0.82	**0.83**	0.97	**0.20**	0.90	0.16	0.91	**0.40**	0.92	**0.41**	0.95
β	**0.50**	0.91	**0.41**	0.92	0.19	0.85	0.15	0.97	**0.36**	0.97	**0.62**	0.97	**0.60**	0.96
n_{riv}	0.08	—	0.06	—	0.03	—	0.18	—	0.12	—	0.08	—	0.07	—
K_{rivV}	0.15	0.63	**0.22**	0.76	0.10	0.75	0.03	0.38	0.09	0.39	0.11	0.38	0.11	0.35
C_{zil}	0.13	0.86	0.10	0.90	0.07	0.91	**0.93**	0.99	**0.79**	0.96	**0.36**	0.94	**0.24**	0.89
A	0.14	—	0.11	—	0.13	—	0.17	—	0.10	—	0.15	—	0.16	—
Θ_{ref}	0.09	—	0.11	—	0.06	—	0.02	—	0.13	—	0.14	—	0.11	—
Θ_w	0.06	—	0.07	—	0.11	—	0.08	—	0.04	—	0.05	—	0.08	—
R_{cmin}	0.11	0.83	0.08	0.91	0.12	0.88	0.08	0.94	0.05	0.94	0.08	0.95	**0.21**	0.96
R_{gl}	0.10	—	0.07	—	0.12	—	0.02	—	0.05	—	0.08	—	0.12	—
h_s	0.10	—	0.07	—	0.12	—	0.13	—	0.14	—	0.06	—	0.06	—
T_{ref}	0.06	—	0.07	—	0.08	—	0.04	—	0.04	—	0.06	—	0.19	—
fx_s	0.17	0.83	0.12	0.92	0.04	0.88	**0.21**	0.98	0.07	0.98	**0.22**	0.98	0.10	0.70
fx_c	0.06	—	0.06	—	0.04	—	0.04	—	0.03	—	0.05	—	0.08	—
k_D	0.06	0.54	0.07	0.60	0.14	0.51	0.01	0.55	0.06	0.55	0.09	0.55	**0.20**	0.61
S	0.11	0.48	0.14	0.55	0.06	0.50	0.14	0.65	**0.26**	0.65	0.19	0.65	**0.26**	0.67

There are 10 parameters, five hydrologic parameters and five land surface parameters, having RMSCs greater than 0.2 with at least one of the observable variables. They are K_V, Θ_e, α, β, K_{rivV}, C_{zil}, R_{cmin}, fx_s, k_D, and S. Those parameters with relatively high distinguishability qualify for single-parameter test to further examine their observability and simplicity.

b. Observability

To test the observability of the model parameters, a group of 10 Flux–PIHM model runs are performed for every parameter with sufficient distinguishability, which results in a total of 100 Flux–PIHM model runs. The RMSDs of observable variables at each time step are calculated. Those time series of RMSDs for different observable variables from different ensemble groups are used to compare the observability of parameters. The comparisons for RMSDs of different observable variables are shown in Fig. 10.

As expected, parameters with high distinguishability all show high observability in the corresponding observable variables, indicated by the relatively high RMSDs in predicted observable variables (Fig. 10). Most of the information from those figures can be deduced from the examinations of the correlations from multiparameter test, except that some parameters with low distinguishability show considerable observability in some of the observable variables. For example, the influence of C_{zil} on model discharge is not distinguishable from other parameters in the multiparameter test (Fig. 2), but C_{zil} produces large RMSDs in model discharge in the single-parameter test (Fig. 10a). The influence of C_{zil} on model discharge is compensated by influences of other model parameters in the multiparameter test.

While hydrologic parameters α and β show strong impacts on land surface variables (Figs. 10d–g), land surface parameters, especially C_{zil} and R_{cmin}, show considerable impacts on hydrologic variables (Figs. 10a–c). In the land surface module, parameters C_{zil} and R_{cmin} influence evapotranspiration the most (Figs. 10f,g). Evapotranspiration extracts soil water and groundwater within the root zone and changes the soil moisture and the water table depth. Although in dry periods (or low flow periods) the influences of land surface parameters on hydrologic variables are not as strong as α and β, those influences change the system response to strong precipitation. During peak flow periods, the RMSDs in Q, WTD, and SWC produced by C_{zil} and R_{cmin} are comparable to those produced by α and β (Fig. 10a). Especially for the peak event in July, C_{zil} produces the largest RMSD in the discharge peak and influences model discharge the most because this event happened after an extended relatively dry period.

As shown in Fig. 9, the parameters Θ_e, α, and β are the most influential parameters on model discharge. RMSDs are large at discharge peaks (Fig. 10a). Effect of Θ_e is the most significant during discharge peaks, but relatively weak during low flow conditions. The parameter β shows high observability consistently, during both peak flow and low flow periods. For the highest

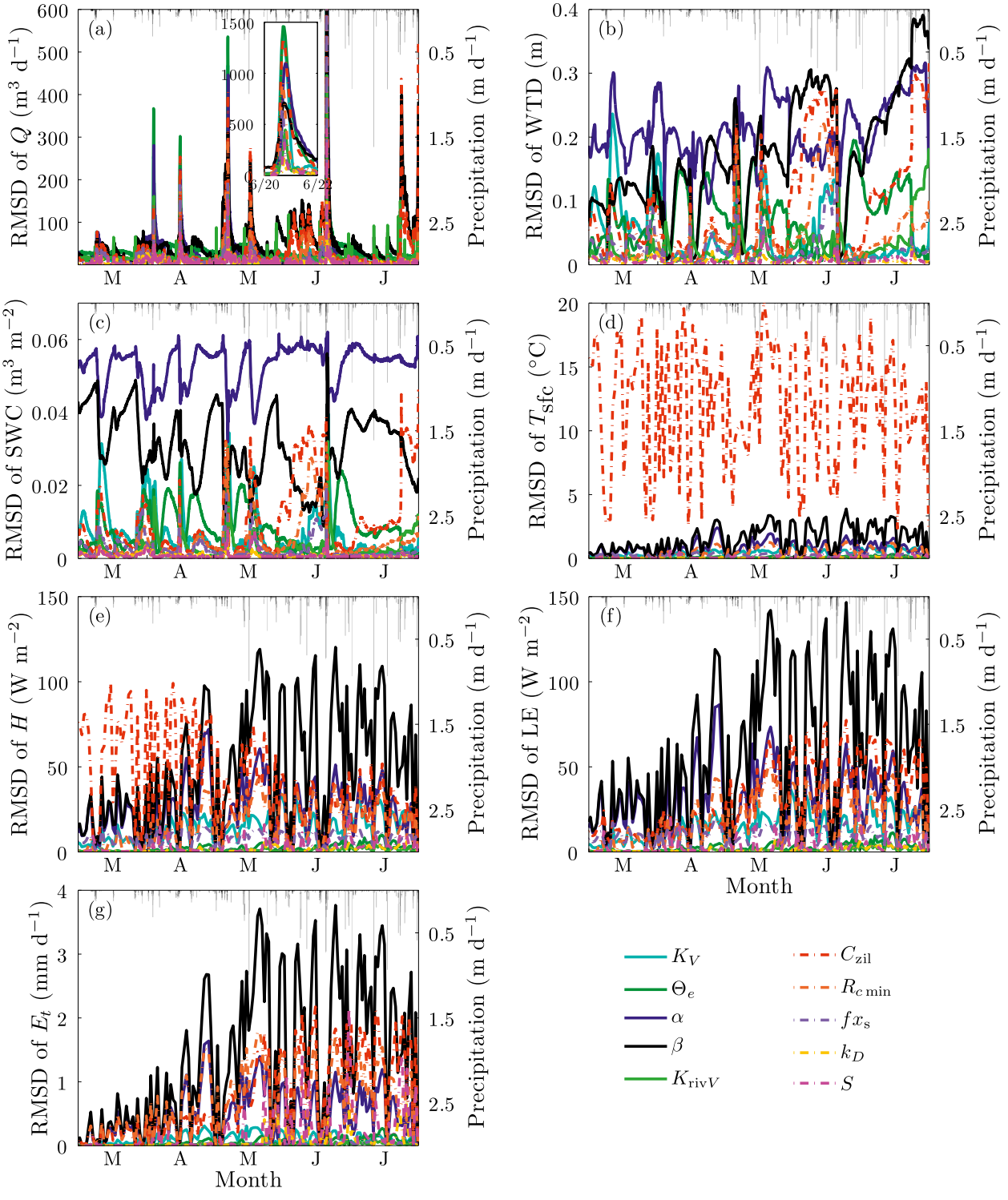

FIG. 10. (a)–(g) RMSDs of observable variables in single-parameter tests. Gray lines indicate strength of precipitation, which is plotted for reference purpose. The inset in (a) highlights the peak discharge event from 20 to 22 October.

peak in June 2009, RMSDs of discharge simulations using different parameters reach as high as $1400\,m^3\,day^{-1}$, which shows the accuracy of the hydrologic model is severely constrained by parameter uncertainties. Besides C_{zil}, land surface parameters R_{cmin} and fx_s show considerable observability in discharge simulations. In spring, during the leaf-off period, the influences of fx_s (related to soil evaporation) are stronger than R_{cmin} (related to transpiration). In summer, when transpiration process dominates the total evapotranspiration, R_{cmin} is more influential than fx_s.

The impacts of model parameters on WTD and SWC at observation wells are similar, except that α is more influential than β in SWC simulations (Figs. 10b,c). From spring to summer, the impacts of land surface parameters get stronger on WTD and SWC. Because of their roles in groundwater recharge, K_V and K_{rivV} also show relatively strong influences on the simulations of WTD and SWC.

The impact of C_{zil} on midday surface skin temperature is far more significant than any other parameter (Fig. 10d). The RMSDs caused by different C_{zil} reach 20°C, while the RMSDs caused by other parameters are always below 5°C. RMSDs of T_{sfc} are larger in summer and in dry periods, when T_{sfc} is relatively higher and smaller in spring and in wet periods, when T_{sfc} is relatively lower.

The impact of C_{zil} on midday sensible heat flux is the most significant in spring (Fig. 10e). But the RMSDs of sensible heat flux caused by different C_{zil} values decrease in summer because the magnitude of sensible heat flux drops. In contrast, observability of hydrologic parameters increases from spring to summer. This is because the Bowen ratio is small in summer and latent heat flux dominates the surface energy balance. Hydrologic parameters then have stronger influences on sensible heat flux via their impacts on evapotranspiration.

For midday latent heat flux and transpiration, RMSDs caused by different parameters are small in spring, when latent heat flux is small, and large in summer, when latent heat flux is large (Fig. 10f). Hydrologic parameters α and β and land surface parameters C_{zil} and R_{cmin} are the most influential parameters, especially β. The parameter S shows relatively high observability on latent heat flux and transpiration during wet periods, when canopy is wet and canopy evaporation occurs.

The RMSCs between the 10 model parameters and the observable variables in single-parameter tests are calculated and presented in Table 2 to be compared with the RMSCs in the multiparameter test. For each pair of parameter and state variable, the RMSC in single-parameter tests is always higher than the RMSC in the multiparameter tests, which implies strong interaction between model parameters.

Three hydrologic parameters and three land surface parameters are chosen for simplicity testing as a result of the distinguishability and observability tests. The inclusion of hydrologic parameters α and β is straightforward. The effective porosity, Θ_e, is chosen because of its strong impact of discharge peaks, the accurate prediction of which is a critical criterion of hydrologic models. Selection of land surface parameter C_{zil} is also straightforward. The parameter R_{cmin} is chosen because it shows high observability in both hydrologic and land surface variables and because it has reasonable distinguishability. The other land surface parameter selected is S, because of its effect on evapotranspiration and discharge during wet periods.

c. Simplicity

For those six parameters with high distinguishability and observability, their simplicity is examined next. Both multiparameter test results and single-parameter test results are used. To test the simplicity, the observable variables from all model runs are plotted as functions of the model parameters. One observable variable is selected for each parameter in the simplicity examination. For parameters Θ_e and β, the variable Q is selected; for α, SWC is picked; for C_{zil}, T_{sfc} is examined; and for R_{cmin} and S, E_t is plotted. Examinations of distinguishability and observability imply that the relationship between variables and parameters could be different in wet (high flow, wet canopy) and dry (low flow, dry canopy) periods. Therefore, simplicity needs to be examined for both wet and dry periods. Two midday time steps are chosen to represent wet and dry periods. The first time chosen is 1700 UTC 20 June 2009, which represents the wet period, including high flow condition, and a wet canopy. It rained almost continuously from 1300 UTC 17 June to 0000 UTC 21 June. The observed highest discharge peak during the whole simulation period occurs around 1800 UTC 20 June. Because of the continuous precipitation, the canopy is wet at this time step. The second time step chosen is 1700 UTC 11 July 2009, which represents the dry period, including low flow condition, and a dry canopy. The period from the beginning of July to 11 July is relatively dry. For the 48 h prior to 1700 UTC 11 July, there has been no precipitation, and the canopy is dry. Relations between different observable variables and different model parameters are presented in Figs. 11 and 12.

Figures 11 and 12 show that for both wet and dry periods, those six parameters show high simplicity in their corresponding observable variables. Except for Q–β in the wet period and E_t–S in the dry period, the other observable variables change monotonically with the change of parameter values in both wet and dry periods,

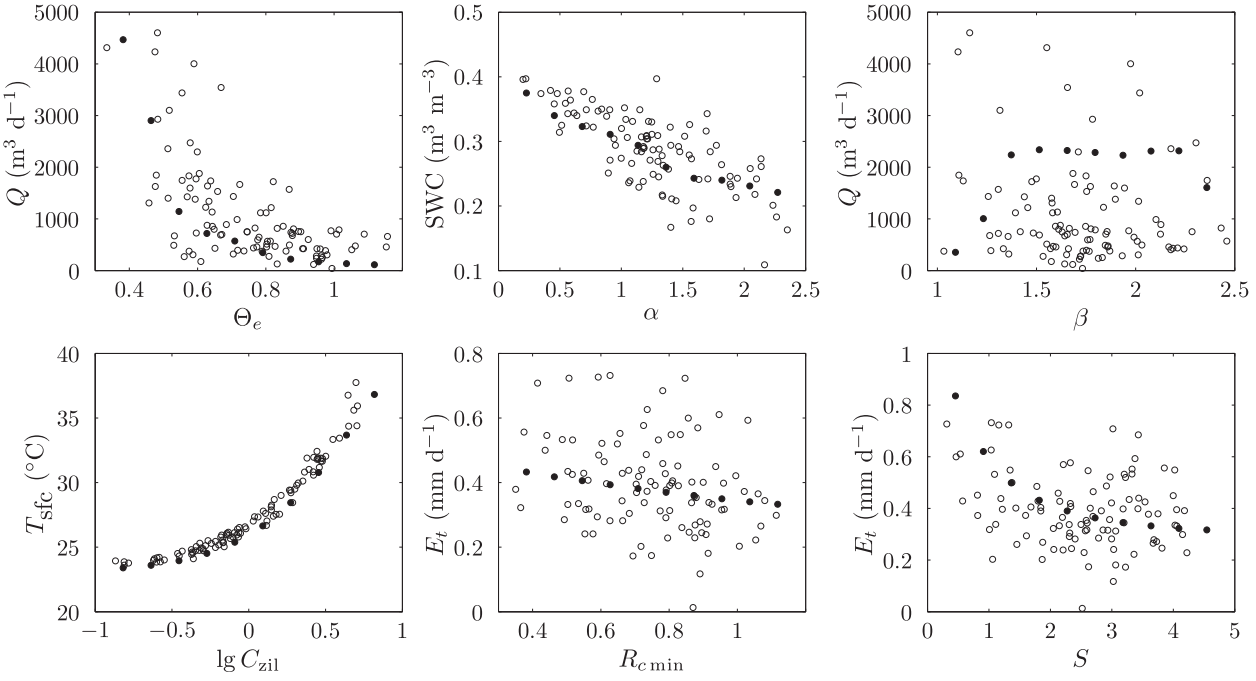

FIG. 11. Flux–PIHM observable variables at 1700 UTC 20 Jun 2009 plotted as functions of model parameters. Circles are from the multiparameter test and dots are from the single-parameter tests.

which shows good linearity of the model. For most of the parameter–variable pairs, the trends in the multiparameter test and the single-parameter tests are similar. The Q–β relationship at 1700 UTC 20 June is not clear. The low simplicity of β in model discharge at this time step suggests that finding an optimal β value using discharge prediction at this time step might be difficult. We note that at the selected dry time step, discharge

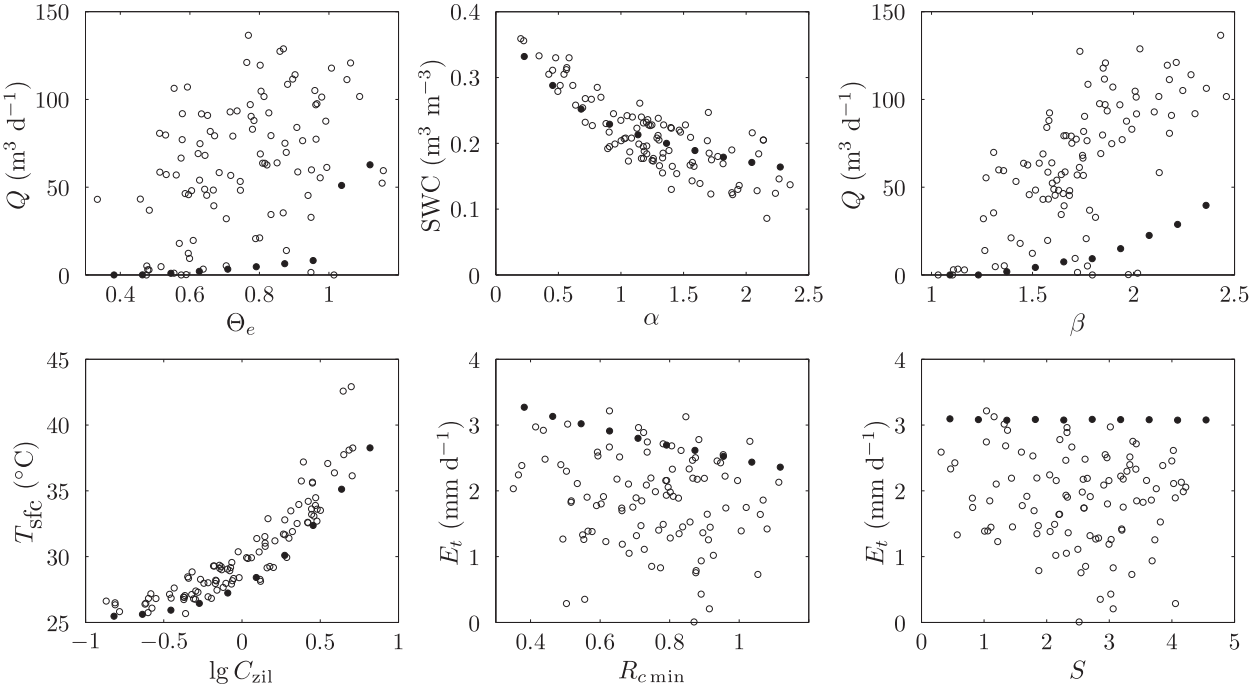

FIG. 12. As in Fig. 11, but at 1700 UTC 11 Jul 2009.

increases monotonically with the increase of β. Given that β shows high observability and distinguishability in multiple observable variables and given the high simplicity at low flow period, it is feasible to find an optimal value for β when relatively long-term or multistate observations are used. As for E_t–S at 1700 UTC 11 July, transpiration is not affected by S (Fig. 12). This is because the canopy is dry and S is not in effect. At the wet time step, however, S shows good simplicity in E_t (Fig. 11).

At the peak flow period, Q decreases monotonically and smoothly with the increase of Θ_e (Fig. 11). At the low flow period, Q increases with the increase of Θ_e (Fig. 12). The different effects of Θ_e in peak flow and low flow are also found in the correlation between Q and Θ_e in the multiparameter test (Fig. 2), which shows Q and Θ_e are negatively correlated at peak flows but positively correlated during low flow periods. For the other parameters, effects in those corresponding observable variables are similar in both dry and wet periods. The chosen observable variables vary monotonically and smoothly with the change of those parameter values.

Examinations of parameter distinguishability, observability, and simplicity show that Flux–PIHM hydrologic parameters Θ_e, α, and β, and land surface parameters C_{zil}, R_{cmin}, and S have relatively high identifiability. It is expected that those six parameters can be estimated effectively using EnKF.

6. Discussion and conclusions

SA is a vital step toward successful parameter estimation. In this paper, SA for Flux–PIHM model parameters is carried out under the framework provided by Nielsen-Gammon et al. (2010). Among all test methods, the evaluation of the correlation between model parameters and observable variables is the most critical test. The correlation coefficients imply parameter distinguishability. Results show that parameters with high distinguishability always have high observability, because their impacts on the system cannot be compensated by the effects of other parameters. Moreover, because the correlation coefficient represents linear dependence, a high correlation coefficient also suggests highly linear dependence and hence simplicity.

The SA reveals that the land surface hydrologic model is very sensitive to parameter values. For the discharge peak in June 2009, the observed discharge rate is $1860\,\mathrm{m^3\,day^{-1}}$, but the single-parameter test RMSDs of the discharge simulations can be as large as $1400\,\mathrm{m^3\,day^{-1}}$ for some model parameters. The RMSDs of midday surface skin temperature simulations are as large as 20°C in the single-parameter test for C_{zil}. Those results indicate that parameter uncertainties produce large uncertainties in hydrologic and land surface simulations.

The SA results show that parameters α, β, and C_{zil} are the most identifiable among the 20 tested parameters. The van Genuchten parameters α and β are highly identifiable in both hydrologic predictions and land surface variable predictions. The Zilitinkevich parameter C_{zil} is highly distinguishable in land surface variables. Although distinguishability of C_{zil} in hydrologic variables is relatively low, observability of C_{zil} is considerably high in hydrologic variables. Anderton et al. (2002) and Christiaens and Feyen (2002) performed SA for different physically based, distributed hydrologic models. Their results showed that model predictions of discharge and soil moisture are very sensitive to the values of van Genuchten parameters. Anderton et al. (2002) found that β is the most critical parameter for the prediction of total discharge and typical autumn runoff events, while α is more important for typical winter runoff events. Christiaens and Feyen (2002) stated that α has the highest influence on the prediction of discharge. The different conclusions might be caused by the different wetness conditions of watersheds chosen in those studies. Our results show that both α and β have strong impacts on discharge and are generally consistent with those studies. Chen et al. (1997) tested the impact of atmospheric surface layer parameterization on a mesoscale atmospheric model. They found that the values of C_{zil} have a strong impact on surface heat fluxes and land surface temperature, which agrees with our results.

Examinations of parameter distinguishability and observability indicate that the land surface and the subsurface are coupled systems in Flux–PIHM. In Flux–PIHM, the subsurface and land surface are linked together by exchanging soil moisture and evapotranspiration information. The subsurface (hydrologic) component provides soil moisture information for the land surface component, while the land surface component provides evapotranspiration rate for the subsurface component. Hydrologic parameters, especially the van Genuchten parameters, have significant influence on land surface simulations through their impacts on soil moisture simulations. At the same time, land surface parameters, especially C_{zil} and R_{cmin} have considerable impacts on discharge, groundwater level, and soil moisture simulations through their influences on evapotranspiration. In summer, the observable hydrologic variable RMSDs caused by land surface parameters and the observable land surface variable RMSDs caused by hydrologic parameters are higher than in spring. This suggests that the interaction between the land surface and the subsurface is especially strong in summer, when evapotranspiration is more active than in other seasons. The interaction

between the subsurface and the land surface suggests that accurate forecasting of hydrologic states cannot be made without reasonable descriptions of land surface, and vice versa. This agrees with the finding of Kampf (2006), who stated that the accuracy of discharge prediction depends on accurate simulations of evapotranspiration. It justifies the need for a coupled land surface hydrologic model.

Examination of parameter distinguishability shows that some parameters with high observability in a certain observable variable do not show high distinguishability for the corresponding observable variable in multiparameter test. For example, parameter C_{zil} exhibits high observability in discharge in the single-parameter test (Fig. 10a) but shows low distinguishability in discharge in the multiparameter test (Fig. 2). This is because the impacts of those parameters are compensated by the effects of other model parameters. Model equifinality (Beven 1993) indicates that the parameter interaction within Flux–PIHM is strong. Parameter estimation is essentially an inverse problem, which converts observed variables into information about model parameters (Moradkhani and Sorooshian 2008). The equifinality and parameter interaction add extra difficulties for parameter estimation. The more observed variables we have, the better chance there is to overcome the difficulties brought by equifinality. Using multiple types of observations for calibration could provide important constraints for parameter estimation.

Results show that parameter identifiability depends on seasonality and canopy wetness. Identifiability of several parameters, for example, K_{infV}, K_V, α, β, C_{zil}, T_{ref} and fx_s, shows seasonal variation. Similar seasonality in parameter sensitivity has also been found in Anderton et al. (2002) and Christiaens and Feyen (2002).

The examination of parameter simplicity (Figs. 11, 12) reveals that the key parameters show good simplicity, that is, model predictions vary smoothly with the change of parameter values, except when some parameters are near to the boundaries of their plausible ranges. It indicates that the model has strong linearity. Therefore, we believe that the choice of the Gaussian mean and the standard deviation in the multiparameter test does not affect the sensitivity results dramatically.

It is important to point out that the examinations of identifiability are made in the context of the selected parameter range and parameter distribution. It is highly possible that the identifiability of parameters becomes different if different ranges are selected; however, the selected ranges are defensible for this site (Table 1). The hydrologic parameters may show stronger distinguishability and observability than the land surface parameters (Fig. 9) because the hydrologic parameters are more weakly constrained and thus have larger ranges than the land surface parameters.

We note that the results presented here are likely to be dependent upon the SA method that we have chosen and to ignore the potential correlation among different input parameters. We have also utilized methods that are best suited to models whose dependence on parameters is relatively linear. An analysis of this model with alternative SA methods, particularly methods that focus on nonlinear behavior of parameter variations, could lead to different parameter rankings and would advance our understanding of this modeling system. Our results do suggest, however, that this model is sufficiently linear that our parameter rankings should provide effective for implementing EnKF parameter estimation.

Six Flux–PIHM parameters are selected based on the examinations of distinguishability, observability, and simplicity and are expected to be estimated effectively by EnKF. Those parameters are the van Genuchten parameters α and β, the effective porosity Θ_e, the Zilitinkevich parameter C_{zil}, the canopy minimum stomatal resistance R_{cmin}, and the reference canopy water capacity S. Among them, α, β, and C_{zil} are the most identifiable parameters.

Acknowledgments. This research was supported by the National Oceanic and Atmospheric Administration through Grant NA10OAR4310166 and the National Science Foundation Susquehanna Shale Hills Critical Zone Observatory project through Grant EAR 0725019.

REFERENCES

Aksoy, A., F. Zhang, and J. W. Nielsen-Gammon, 2006: Ensemble-based simultaneous state and parameter estimation in a two-dimensional sea-breeze model. *Mon. Wea. Rev.,* **134,** 2951–2970, doi:10.1175/MWR3224.1.

Anderson, M. C., J. M. Norman, G. R. Diak, W. P. Kustas, and J. R. Mecikalski, 1997: A two-source time-integrated model for estimating surface fluxes using thermal infrared remote sensing. *Remote Sens. Environ.,* **60,** 195–216, doi:10.1016/S0034-4257(96)00215-5.

Anderton, S., J. Latron, and F. Gallart, 2002: Sensitivity analysis and multi-response, multi-criteria evaluation of a physically based distributed model. *Hydrol. Processes,* **16,** 333–353, doi:10.1002/hyp.336.

Beven, K., 1993: Prophecy, reality and uncertainty in distributed hydrological modelling. *Adv. Water Resour.,* **16,** 41–51, doi:10.1016/0309-1708(93)90028-E.

——, and A. Binley, 1992: The future of distributed models: Model calibration and uncertainty prediction. *Hydrol. Processes,* **6,** 279–298, doi:10.1002/hyp.3360060305.

Bras, R. L., 1990: *Hydrology: An Introduction to Hydrologic Science.* Addison-Wesley, 643 pp.

Cammalleri, C., and G. Ciraolo, 2012: State and parameters update in a coupled energy/hydrologic balance model using ensemble Kalman filtering. *J. Hydrol.,* **416–417,** 171–181, doi:10.1016/j.jhydrol.2011.11.049.

Campolongo, F., and A. Saltelli, 1997: Sensitivity analysis of an environmental model: An application of different analysis methods. *Reliab. Eng. Syst. Saf.,* **57,** 49–69, doi:10.1016/S0951-8320(97)00021-5.

Chen, F., and J. Dudhia, 2001: Coupling an advanced land surface–hydrology model with the Penn State–NCAR MM5 modeling system. Part I: Model implementation and sensitivity. *Mon. Wea. Rev.,* **129,** 569–585, doi:10.1175/1520-0493(2001)129<0569:CAALSH>2.0.CO;2.

——, Z. Janjić, and K. Mitchell, 1997: Impact of atmospheric-surface layer parameterizations in the new land surface scheme of the NCEP mesoscale Eta numerical model. *Bound.-Layer Meteor.,* **85,** 391–421, doi:10.1023/A:1000531001463.

Christiaens, K., and J. Feyen, 2002: Use of sensitivity and uncertainty measures in distributed hydrological modeling with an application to the MIKE SHE model. *Water Resour. Res.,* **38,** 1169, doi:10.1029/2001WR000478.

Confalonieri, R., G. Bellocchi, S. Bregaglio, M. Donatelli, and M. Acutis, 2010: Comparison of sensitivity analysis techniques: A case study with the rice model WARM. *Ecol. Modell.,* **221,** 1897–1906, doi:10.1016/j.ecolmodel.2010.04.021.

Crow, W. T., and E. F. Wood, 2003: The assimilation of remotely sensed soil brightness temperature imagery into a land surface model using ensemble Kalman filtering: A case study based on ESTAR measurements during SGP97. *Adv. Water Resour.,* **26,** 137–149, doi:10.1016/S0309-1708(02)00088-X.

Cukier, R. I., C. M. Fortuin, K. E. Shuler, A. G. Petschek, and J. H. Schaibly, 1973: Study of the sensitivity of coupled reaction systems to uncertainties in rate coefficients. I. Theory. *J. Chem. Phys.,* **59,** 3873–3878, doi:10.1063/1.1680571.

——, J. H. Schaibly, and K. E. Shuler, 1975: Study of the sensitivity of coupled reaction systems to uncertainties in rate coefficients. III. Analysis of the approximations. *J. Chem. Phys.,* **63,** 1140–1149, doi:10.1063/1.431440.

——, H. B. Levine, and K. E. Shuler, 1978: Nonlinear sensitivity analysis of multiparameter model systems. *J. Comput. Phys.,* **26,** 1–42, doi:10.1016/0021-9991(78)90097-9.

Cullmann, J., V. Mishra, and R. Peters, 2006: Flow analysis with WaSiM-ETH—Model parameter sensitivity at different scales. *Adv. Geosci.,* **9,** 73–77, doi:10.5194/adgeo-9-73-2006.

Demaria, E. M., B. Nijssen, and T. Wagener, 2007: Monte Carlo sensitivity analysis of land surface parameters using the Variable Infiltration Capacity model. *J. Geophys. Res.,* **112,** D11113, doi:10.1029/2006JD007534.

Dickinson, R. E., A. Henderson-Sellers, and P. J. Kennedy, 1993: Biosphere-Atmosphere Transfer Scheme (BATS) version 1e as coupled to the NCAR Community Climate Model. NCAR Tech. Note TN-387STR, National Center for Atmospheric Research, Boulder, CO, 72 pp. [Available online at http://nldr.library.ucar.edu/repository/assets/technotes/TECH-NOTE-000-000-000-198.pdf.]

Eckhardt, K., and J. G. Arnold, 2001: Automatic calibration of a distributed catchment model. *J. Hydrol.,* **251,** 103–109, doi:10.1016/S0022-1694(01)00429-2.

Ek, M. B., K. Mitchell, Y. Lin, E. Rogers, P. Grummann, V. Koren, G. Gayno, and J. Tarpley, 2003: Implementation of Noah land surface model advances in the National Centers for Environmental Prediction operational Mesoscale Eta Model. *J. Geophys. Res.,* **108,** 8851, doi:10.1029/2002JD003296.

Evensen, G., 1994: Sequential data assimilation with a nonlinear quasi-geostrophic model using Monte Carlo methods to forecast error statistics. *J. Geophys. Res.,* **99** (C5), 10 143–10 162, doi:10.1029/94JC00572.

Franchini, M., 1996: Use of a genetic algorithm combined with a local search method for the automatic calibration of conceptual rainfall-runoff models. *Hydrol. Sci. J.,* **41,** 21–39, doi:10.1080/02626669609491476.

Freer, J., K. Beven, and B. Ambroise, 1996: Bayesian estimation of uncertainty in runoff prediction and the value of data: An application of the GLUE approach. *Water Resour. Res.,* **32,** 2161–2173, doi:10.1029/95WR03723.

Frey, H. C., and S. R. Patil, 2002: Identification and review of sensitivity analysis methods. *Risk Anal.,* **22,** 553–578, doi:10.1111/0272-4332.00039.

Gupta, H. V., L. A. Bastidas, S. Sorooshian, W. J. Shuttleworth, and Z.-L. Yang, 1999: Parameter estimation of a land surface scheme using multicriteria methods. *J. Geophys. Res.,* **104** (D16), 19 491–19 503, doi:10.1029/1999JD900154.

Gupta, V. K., and S. Sorooshian, 1985: The relationship between data and the precision of parameter estimates of hydrologic models. *J. Hydrol.,* **81,** 57–77, doi:10.1016/0022-1694(85)90167-2.

Hacker, J. P., and C. Snyder, 2005: Ensemble Kalman filter assimilation of fixed screen-height observations in a parameterized PBL. *Mon. Wea. Rev.,* **133,** 3260–3275, doi:10.1175/MWR3022.1.

Hall, J. W., S. A. Boyce, Y. Wang, R. J. Dawson, S. Tarantola, and A. Saltelli, 2009: Sensitivity analysis for hydraulic models. *J. Hydraul. Eng.,* **135,** 959–969, doi:10.1061/(ASCE)HY.1943-7900.0000098.

Helton, J. C., J. D. Johnson, C. J. Sallaberry, and C. B. Storlie, 2006: Survey of sampling-based methods for uncertainty and sensitivity analysis. *Reliab. Eng. Syst. Saf.,* **91,** 1175–1209, doi:10.1016/j.ress.2005.11.017.

Henriksen, H. J., L. Troldborg, P. Nyegaard, T. O. Sonnenborg, J. C. Refsgaard, and B. Madsen, 2003: Methodology for construction, calibration and validation of a national hydrological model for Denmark. *J. Hydrol.,* **280,** 52–71, doi:10.1016/S0022-1694(03)00186-0.

Hornberger, G. M., and R. C. Spear, 1981: Approach to the preliminary analysis of environmental systems. *J. Environ. Manage.,* **12,** 7–18.

Hu, X.-M., F. Zhang, and J. W. Nielsen-Gammon, 2010: Ensemble-based simultaneous state and parameter estimation for treatment of mesoscale model error: A real-data study. *Geophys. Res. Lett.,* **37,** L08802, doi:10.1029/2010GL043017.

Jackson, C., Y. Xia, M. K. Sen, and P. L. Stoffa, 2003: Optimal parameter and uncertainty estimation of a land surface model: A case study using data from Cabauw, Netherlands. *J. Geophys. Res.,* **108,** 4583, doi:10.1029/2002JD002991.

Jacques, J., C. Lavergne, and N. Devictor, 2006: Sensitivity analysis in presence of model uncertainty and correlated inputs. *Reliab. Eng. Syst. Saf.,* **91,** 1126–1134, doi:10.1016/j.ress.2005.11.047.

Kalman, R. E., 1960: A new approach to linear filtering and prediction problems. *J. Basic Eng.,* **82,** 35–45, doi:10.1115/1.3662552.

Kampf, S. K., 2006: Towards improved representations of hydrologic processes: Linking integrated and distributed hydrologic measurements to a physically-based model for a planar hillslope plot. Water Resources Series Tech. Rep. 183, Department of Civil and Environal Engineering, University of Washington, Seattle, WA, 213 pp. [Available online at http://depts.washington.edu/uwbg/research/Burges/_WRS183-Kampf-2006.pdf.]

Kollat, J. B., and P. M. Reed, 2006: Comparing state-of-the-art evolutionary multi-objective algorithms for long-term groundwater monitoring design. *Adv. Water Resour.,* **29,** 792–807, doi:10.1016/j.advwatres.2005.07.010.

Kumar, M., 2009: Toward a hydrologic modeling system. Ph.D. thesis, The Pennsylvania State University, 251 pp.

Lin, H., 2006: Temporal stability of soil moisture spatial pattern and subsurface preferential flow pathways in the Shale Hills catchment. *Vadose Zone J.,* **5,** 317–340, doi:10.2136/vzj2005.0058.

——, and X. Zhou, 2008: Evidence of subsurface preferential flow using soil hydrologic monitoring in the Shale Hills catchment. *Eur. J. Soil Sci.,* **59,** 34–49, doi:10.1111/j.1365-2389.2007.00988.x.

Lü, H., T. Hou, R. Horton, Y. Zhu, X. Chen, Y. Jia, W. Wang, and X. Fu, 2013: The streamflow estimation using the Xinanjiang rainfall runoff model and dual state-parameter estimation method. *J. Hydrol.,* **480,** 102–114, doi:10.1016/j.jhydrol.2012.12.011.

Massmann, C., and H. Holzmann, 2012: Analysis of the behavior of a rainfall-runoff model using three global sensitivity analysis methods evaluated at different temporal scales. *J. Hydrol.,* **475,** 97–110, doi:10.1016/j.jhydrol.2012.09.026.

Moradkhani, H., and S. Sorooshian, 2008: General review of rainfall-runoff modeling: Model calibration, data assimilation, and uncertainty analysis. *Hydrological Modelling and the Water Cycle,* S. Sorooshian et al., Eds., Springer, Water Science and Technology Library, Vol. 63, 1–24.

——, ——, H. V. Gupta, and P. R. Houser, 2005: Dual state-parameter estimation of hydrological models using ensemble Kalman filter. *Adv. Water Resour.,* **28,** 135–147, doi:10.1016/j.advwatres.2004.09.002.

Morris, M. D., 1991: Factorial sampling plans for preliminary computational experiments. *Technometrics,* **33** (2), 161–174, doi:10.1080/00401706.1991.10484804.

Nielsen-Gammon, J. W., X. M. Hu, F. Zhang, and J. E. Pleim, 2010: Evaluation of planetary boundary layer scheme sensitivities for the purpose of parameter estimation. *Mon. Wea. Rev.,* **138,** 3400–3417, doi:10.1175/2010MWR3292.1.

Pappenberger, F., K. J. Beven, M. Ratto, and P. Matgen, 2008: Multi-method global sensitivity analysis of flood inundation models. *Adv. Water Resour.,* **31,** 1–14, doi:10.1016/j.advwatres.2007.04.009.

Pokhrel, P., and H. V. Gupta, 2010: On the use of spatial regularization strategies to improve calibration of distributed watershed models. *Water Resour. Res.,* **46,** W01505, doi:10.1029/2009WR008066.

Prihodko, L., A. S. Denning, N. P. Hanan, I. Baker, and K. J. Davis, 2008: Sensitivity, uncertainty and time dependence of parameters in a complex land surface model. *Agric. For. Meteor.,* **148,** 268–287, doi:10.1016/j.agrformet.2007.08.006.

Qu, Y., 2004: An integrated hydrologic model for multi-process simulation using semi-discrete finite volume approach. Ph.D. thesis, The Pennsylvania State University, 143 pp. [Available online at http://www.pihm.psu.edu/Downloads/Articles/qu_thesis.pdf.]

——, and C. J. Duffy, 2007: A semidiscrete finite volume formulation for multiprocess watershed simulation. *Water Resour. Res.,* **43,** W08419, doi:10.1029/2006WR005752.

Reichle, R. H., S. V. Kumar, S. P. P. Mahanama, R. D. Koster, and Q. Liu, 2010: Assimilation of satellite-derived skin temperature observations into land surface models. *J. Hydrometeor.,* **11,** 1103–1122, doi:10.1175/2010JHM1262.1.

Reusser, D. E., W. Buytaert, and E. Zehe, 2011: Temporal dynamics of model parameter sensitivity for computationally expensive models with the Fourier amplitude sensitivity test. *Water Resour. Res.,* **47,** W07551, doi:10.1029/2010WR009947.

Salehi, F., S. O. Prasher, S. Amin, A. Madani, S. J. Jebelli, H. S. Ramaswamy, C. Tan, and C. F. Drury, 2000: Prediction of annual nitrate-N losses in drain outflows with artificial neural networks. *Trans. ASAE,* **43,** 1137–1143, doi:10.13031/2013.3006.

Saltelli, A., S. Tarantola, and F. Campolongo, 2000: Sensitivity analysis as an ingredient of modeling. *Stat. Sci.,* **15,** 377–395, doi:10.1214/ss/1009213004.

——, M. Ratto, S. Tarantola, and F. Campolongo, 2005: Sensitivity analysis for chemical models. *Chem. Rev.,* **105,** 2811–2828, doi:10.1021/cr040659d.

——, ——, ——, and ——, 2006: Sensitivity analysis practices: Strategies for model-based inference. *Reliab. Eng. Syst. Saf.,* **91,** 1109–1125, doi:10.1016/j.ress.2005.11.014.

Sellers, P. J., W. J. Shuttleworth, J. L. Dorman, A. Dalcher, and J. M. Roberts, 1989: Calibrating the simple biosphere model for Amazonian tropical forest using field and remote sensing data. Part I: Average calibration with field data. *J. Appl. Meteor.,* **28,** 727–759, doi:10.1175/1520-0450(1989)028<0727:CTSBMF>2.0.CO;2.

Shi, Y., K. J. Davis, C. J. Duffy, and X. Yu, 2013a: Development of a coupled land surface hydrologic model and evaluation at a critical zone observatory. *J. Hydrometeor.,* **14,** 1401–1420, doi:10.1175/JHM-D-12-0145.1.

Sobol', I. M., 1993: Sensitivity estimates for nonlinear mathematical models. *Math. Modell. Comput. Exp.,* **1,** 407–414.

Sorooshian, S., Q. Duan, and V. K. Gupta, 1993: Calibration of rainfall-runoff models: Application of global optimization to the Sacramento Soil Moisture Accounting Model. *Water Resour. Res.,* **29,** 1185–1194, doi:10.1029/92WR02617.

Sun, X. Y., L. T. H. Newham, B. F. W. Croke, and J. P. Norton, 2012: Three complementary methods for sensitivity analysis of a water quality model. *Environ. Modell. Software,* **37,** 19–29, doi:10.1016/j.envsoft.2012.04.010.

Tang, Y., P. Reed, and T. Wagener, 2006: How effective and efficient are multiobjective evolutionary algorithms at hydrologic model calibration? *Hydrol. Earth Syst. Sci.,* **10,** 289–307, doi:10.5194/hess-10-289-2006.

——, ——, ——, and K. Van Werkhoven, 2007: Comparing sensitivity analysis methods to advance lumped watershed model identification and evaluation. *Hydrol. Earth Syst. Sci.,* **11,** 793–817, doi:10.5194/hess-11-793-2007.

van Genuchten, M. T., 1980: A closed-form equation for predicting the hydraulic conductivity of unsaturated soils. *Soil Sci. Soc. Amer. J.,* **44,** 892–898, doi:10.2136/sssaj1980.03615995004400050002x.

Vrugt, J. A., H. V. Gupta, L. A. Bastidas, W. Bouten, and S. Sorooshian, 2003: Effective and efficient algorithm for multiobjective optimization of hydrologic models. *Water Resour. Res.,* **39,** 1214, doi:10.1029/2002WR001746.

Wagener, T., N. McIntyre, M. J. Lees, H. S. Wheater, and H. V. Gupta, 2003: Towards reduced uncertainty in conceptual rainfall-runoff modelling: Dynamic identifiability analysis. *Hydrol. Processes,* **17,** 455–476, doi:10.1002/hyp.1135.

Wallner, M., and Coauthors, 2012: Evaluation of different calibration strategies for large scale continuous hydrological modelling. *Adv. Geosci.,* **31,** 67–74, doi:10.5194/adgeo-31-67-2012.

Xia, Y., A. J. Pitman, H. V. Gupta, M. Leplastrier, A. Henderson-Sellers, and L. A. Bastidas, 2002: Calibrating a land surface model of varying complexity using multicriteria methods and the Cabauw dataset. *J. Hydrometeor.,* **3,** 181–194, doi:10.1175/1525-7541(2002)003<0181:CALSMO>2.0.CO;2.

Xie, X., and D. Zhang, 2010: Data assimilation for distributed hydrological catchment modeling via ensemble

Kalman filter. *Adv. Water Resour.,* **33,** 678–690, doi:10.1016/j.advwatres.2010.03.012.

Yu, X., G. Bhatt, C. Duffy, and Y. Shi, 2013: Parameterization for distributed watershed modeling using national data and evolutionary algorithm. *Comput. Geosci.,* **58,** 80–90, doi:10.1016/j.cageo.2013.04.025.

Zilitinkevich, S. S., 1995: Non-local turbulent transport: Pollution dispersion aspects of coherent structure of convective flows. *Air Pollution Theory and Simulation,* Vol. 1, *Air Pollution III,* H. Power, N. Moussiopoulos, and C. A. Brebbia, Eds., Computational Mechanics Publications, 53–60.

Zupanski, D., and M. Zupanski, 2006: Model error estimation employing an ensemble data assimilation approach. *Mon. Wea. Rev.,* **134,** 1337–1354, doi:10.1175/MWR3125.1.